National Aeronautics and Space Administration

Langley Research Center

Hampton, Virginia 23681-2199

Cloud – Aerosol LIDAR and Infrared Pathfinder Satellite Observations (CALIPSO)

Data Description and Quality Summary

Lidar Level 1B Data

DOI: https://doi.org/10.5067/CALIOP/CALIPSO/CAL_LID_L1_Data_Description_Document_V5

Cloud – Aerosol LIDAR and Infrared Pathfinder Satellite Observations

Data Description and Quality Summary

Lidar Level 1B Data

Primary Authors

Mark Vaughan, Michael Pitts, Charles Trepte, David Winker, Brian Getzewich, Jason Tackett, Xia Cai
NASA Langley Research Center
Hampton, Virginia 23681-2199

Jacques Pelon
LATMOS/IPSL, Université Pierre et Marie Curie
75252 Paris Cedex 5 (France)

Anne Garnier, Jayanta Kar, Kam-Pui Lee
Analytical Mechanics Associates (AMA)
21 Enterprise Parkway, Hampton, Virginia 23666

Timothy Murray, Sharon Rodier
ADNET Systems, Inc.
6720B Rockledge Drive, Suite #504, Bethesda, Maryland 20817

Robert Ryan
Coherent Applications, Inc. – Psionic LLC
1100 Exploration Way, Hampton, Virginia 23666

January 21, 2026

CALIPSO Lidar Level 1B Data Description Document

Version 5.00

Final Data Version: 5.00
Final Data Release Date: October 1, 2025
Final Data Date Range: June 13, 2006, to June 30, 2023

Introduction

The V5.0 CALIPSO Lidar Level 1B (L1B) data products report vertical profiles of calibrated and geolocated laser backscatter, including total attenuated backscatter coefficients at 532 nm and 1064 nm and 532 nm perpendicular channel attenuated backscatter coefficients. Data are distributed in Hierarchical Data Format Version 4 (HDF4). Due to the very different noise characteristics in CALIOP daytime and nighttime measurements, these HDF4 files are partitioned into day-night segments (i.e., granules) corresponding to approximately one-half orbit each. Between altitudes of -0.5 km to 8.2 km above mean sea level (AMSL), CALIOP profile data are reported at single shot resolution. At higher altitudes, where data are averaged onboard the satellite, the averaged profiles are replicated as necessary to generate a pseudo-single shot data product. The L1B files report data from all nominal science mode measurements, but do not report measurements acquired when the lidar is configured in a diagnostic mode (e.g., boresighting).

The CALIOP Level 1B product also contains a substantial amount of ancillary information, including post processed ephemeris data, celestial data, payload status data, and meteorological profiles (e.g., temperature and pressure) obtained from the Modern-Era Retrospective analysis for Research and Applications, Version 2 (MERRA-2) data set.

The parameters contained in the V5.00 CALIOP Level 1B data product are largely unchanged from the previous version (version 4.51), although the reflectances, reflectance uncertainties, and reflectance calibration coefficient are generated by a thoroughly revamped retrieval. Furthermore, the attributes provided for individual scientific data sets (SDSs) have been revised substantially, greatly improving the "self-documenting" capabilities of the CALIOP data files. A complete list of algorithm and data product content changes is given below in the V5.00 data quality summary.

Table of Contents

Introduction 3
Additional Documentation 8
Glossary and Acronym Dictionary 8
Scientific Data Sets: Measurement Altitudes 10
Lidar_Data_Altitudes 10
Met_Data_Altitudes 11
Scientific Data Sets: Time and Position 11
Profile_Time 11
Profile_UTC_Time 11
Day_Night_Flag 11
Profile_ID 11

Latitude 11
Longitude 12
Scientific Data Sets: Lidar Operating Mode 12
Frame_Number 12
Lidar_Mode 12
Lidar_Submode 12
Laser_Energy_532 13
Laser_Energy_1064 13
Parallel_Amplifier_Gain_532 13
Perpendicular_Amplifier_Gain_532 13
Amplifier_Gain_1064 13
Off_Nadir_Angle 13
Surface_Altitude_Shift 14
Number_Bins_Shift 14
Scientific Data Sets: Surface Information 15
Land_Water_Mask 15
IGBP_Surface_Type 15
Snow_Ice_Surface_Type 16
Surface_Elevation 16
GMAO_Surface_Elevation 16
Scientific Data Sets: Signal Quality 17
Surface_Saturation_Flag_532Par 17
Surface_Saturation_Flag_532Perp 17
Surface_Saturation_Flag_1064 17
Surface_Saturation_Index_532Par 17
Surface_Saturation_Index_532Perp 17
Surface_Saturation_Index_1064 17
Negative_Signal_Anomaly_Index_532Par 17
Negative_Signal_Anomaly_Index_532Perp 17
Negative_Signal_Anomaly_Index_1064 17
Parallel_Background_Monitor_532 18
Perpendicular_Background_Monitor_532 18
Parallel_RMS_Baseline_532 19
Perpendicular_RMS_Baseline_532 19
RMS_Baseline_1064 19
Scientific Data Sets: Calibration Coefficients 19
Calibration_Constant_532 19

Calibration_Constant_Uncertainty_532 20
Calibration_Constant_1064 21
Calibration_Constant_Uncertainty_1064 21
Depolarization_Gain_Ratio_532 21
Depolarization_Gain_Ratio_Uncertainty_532 22
Scientific Data Sets: Backscatter Profiles 22
Total_Attenuated_Backscatter_532 22
Perpendicular_Attenuated_Backscatter_532 23
Attenuated_Backscatter_1064 23
Noise_Scale_Factor_532_Parallel 23
Noise_Scale_Factor_532_Perpendicular 23
Noise_Scale_Factor_1064 23
Scientific Data Sets: Reflectances 24
Parallel_Column_Reflectance_532 24
Perpendicular_Column_Reflectance_532 24
Parallel_Column_Reflectance_Uncertainty_532 24
Perpendicular_Column_Reflectance_Uncertainty_532 24
Reflectance_Calibration_Coefficient_532 24
Reflectance_Calibration_Coefficient_Uncertainty_532 24
Scientific Data Sets: Ancillary Meteorological Data 25
Molecular_Number_Density 25
Ozone_Number_Density 25
Temperature 25
Pressure 25
Relative_Humidity 25
Surface_Wind_Speeds_02m 25
Surface_Wind_Speeds_10m 25
Tropopause_Height 26
Tropopause_Temperature 26
Scientific Data Sets: Quality Assurance 26
QC_Flag 26
QC_Flag_2 27
Scientific Data Sets: Orbital Environment 28
Viewing_Zenith_Angle 28
Viewing_Azimuth_Angle 29
Solar_Zenith_Angle 29
Solar_Azimuth_Angle 29

Scattering_Angle 29
Scientific Data Sets: Spacecraft Position and Attitude 29
Spacecraft_Altitude 29
Spacecraft_Position 29
Spacecraft_Velocity 30
Spacecraft_Attitude 30
Spacecraft_Attitude_Rate 30
Subsatellite_Latitude 30
Subsatellite_Longitude 30
Earth_Sun_Distance 30
Subsolar_Latitude 30
Subsolar_Longitude 31
Metadata Parameters 31
Product_ID 31
Date_Time_at_Granule_Start 31
Date_Time_at_Granule_End 31
Date_Time_at_Granule_Production 31
Number_of_Bad_Profiles 31
Number_of_Good_Profiles 31
Initial_Subsatellite_Latitude 31
Initial_Subsatellite_Longitude 32
Final_Subsatellite_Latitude 32
Final_Subsatellite_Longitude 32
Orbit_Number_at_Granule_Start 32
Orbit_Number_at_Granule_End 32
Orbit_Number_Change_Time 32
Path_Number_at_Granule_Start 32
Path_Number_at_Granule_End 32
Path_Number_Change_Time 32
Ephemeris_Files_Used 32
Attitude_Files_Used 32
GMAO_Files_Used 33
Snow_Ice_Files_Used 33
GEOS_Version 33
Percent_532-parallel_Bad 33
Percent_532-perpendicular_Bad 33
Percent_1064_Bad 33

Percent_532-parallel_Missing 33
Percent_532-perpendicular_Missing 33
Percent_1064_Missing 33
Cal_Region_Top_Altitude_532 33
Cal_Region_Base_Altitude_532 33
Lidar_Data_Altitudes 33
Met_Data_Altitudes 33
Rayleigh Extinction_Cross-section_532 33
Rayleigh_Extinction_Cross-section_1064 33
Rayleigh_Backscatter_Cross-section_1064 34
Ozone_Absorption_Cross-section_532 34
Ozone_Absorption_Cross-section_1064 34
ScatteringRatioIn532NightCalibrationRegion 34
ScatteringRatioIn532NightCalibrationRegionUncertainty 34
MolecularModelUncertainty 34
CirrusBackscatterColorRatio 34
CirrusBackscatterColorRatioUncertainty 34
AutocorrelationCoefficientFile 34
Data Release Information 34
Data Quality Information 35
Data Quality Statement for the Version 5.00 Lidar Level 1B Product 35
Data Quality Statement for the Version 4.51 Lidar Level 1B Product 40
Data Quality Statement for the Version 4.11 Lidar Level 1B Product 45
Data Quality Statement for the Version 4.10 Lidar Level 1B Product 45
Data Quality Statement for the Version 4.00 Lidar Level 1B Product 46
Data Quality Statement for the Version 3.41 Lidar Level 1B Product 52
Data Quality Statement for the Version 3.40 Lidar Level 1B Product 53
Data Quality Statement for the Version 3.30 Lidar Level 1B Product 53
Data Quality Statement for the Version 3.02 Lidar Level 1B Product 53
Data Quality Statement for the Version 3.01 Lidar Level 1B Product 53
Data Quality Statement for the Version 3.00 Lidar Level 1B Product 53
Data Quality Statement for the Version 2.02 Lidar Level 1B Product 54
Data Quality Statement for the Version 2.01 Lidar Level 1B Product 55
Data Quality Statement for the Version 1.22 Lidar Level 1B Product 55
Data Quality Statement for the Version 1.20 Lidar Level 1B Product 56
Data Quality Statement for the Version 1.11 Lidar Level 1B Product 56
Data Quality Statement for the Version 1.10 Lidar Level 1B Product 56

Data Quality Statement for the Transient Response of the 532 nm Detectors 56
Appendix 1: Granules Containing Unusual Off-Nadir Angles 57
Appendix 2: Estimating Random Uncertainties for Attenuated Backscatter Coefficients 59
Appendix 3: Non-ideal Response of the CALIOP 532 nm Detectors 62
References 65

Additional Documentation

Project Documentation

- CALIPSO Data Management Team: CALIPSO Data Products Catalog, PC-SCI-503, Release 5.00.
- Hostetler, C. A., Z. Liu, J. Reagan, M. A. Vaughan, D. M., Winker, M. Osborn, W. A. Hunt, K. A. Powell, and C. Trepte, 2006: CALIOP Algorithm Theoretical Basis Document: Calibration and Level 1 Data Products, PC-SCI-201.01, https://ntrs.nasa.gov/citations/20250006623.
- Winker, D. M., C. A. Hostetler, M. A. Vaughan, and A. H. Omar, 2006: Cloud-Aerosol Lidar with Orthogonal Polarization (CALIOP) Algorithm Theoretical Basis Document Part 1: CALIOP Instrument, and Algorithms Overview, PC-SCI-202 Part 1, Release 2.0, 29 pp., https://ntrs.nasa.gov/citations/20250006626.

Peer-Reviewed Algorithm Papers

- Getzewich, B. J., M. A. Vaughan, W. H. Hunt, M. A. Avery, K. A. Powell, J. L. Tackett, D. M. Winker, J. Kar, K.-P. Lee, and T. Toth, 2018: CALIPSO Lidar Calibration at 532-nm: Version 4 Daytime Algorithm, *Atmos. Meas. Tech.*, **11**, 6309–6326, https://doi.org/10.5194/amt-11-6309-2018.
- Kar, J., M. A. Vaughan, K. P. Lee, J. Tackett, M. Avery, A. Garnier, B. Getzewich, W. Hunt, D. Josset, Z. Liu, P. Lucker, B. Magill, A. Omar, J. Pelon, R. Rogers, T. D. Toth, C. Trepte, J-P. Vernier, D. Winker, and S. Young, 2018: CALIPSO Lidar Calibration at 532 nm: Version 4 Nighttime Algorithm, *Atmos. Meas. Tech.*, **11**, 1459–1479, https://doi.org/10.5194/amt-11-1459-2018.
- Powell, K. A., C. A. Hostetler, Z. Liu, M. A. Vaughan, R. E. Kuehn, W. H. Hunt, K. Lee, C. R. Trepte, R. R. Rogers, S. A. Young, and D. M. Winker, 2009: CALIPSO Lidar Calibration Algorithms: Part I - Nighttime 532 nm Parallel Channel and 532 nm Perpendicular Channel, *J. Atmos. Oceanic Technol.*, **26**, 2015–2033, https://doi.org/10.1175/2009JTECHA1242.1.
- Vaughan, M., A. Garnier, D. Josset, M. Avery, K.-P. Lee, Z. Liu, W. Hunt, J. Pelon, Y. Hu, S. Burton, J. Hair, J. Tackett, B. Getzewich, J. Kar, and S. Rodier, 2019: CALIPSO Lidar Calibration at 1064 nm: Version 4 Algorithm, *Atmos. Meas. Tech.*, **12**, 51–82, https://doi.org/10.5194/amt-12-51-2019.
- Vaughan, M., S. D. Rodier, Z. Liu, A. Garnier, K.-P. Lee, B. Getzewich and S. Zeng, 2023: Correcting CALIOP Polarization Gain Ratios for Diurnal Variations, in Proceedings of the 30th International Laser Radar Conference, Sullivan, J. T. et al., Eds., pp. 691–697, Springer Atmospheric Sciences, Springer, Cham., https://doi.org/10.1007/978-3-031-37818-8_89.

Glossary and Acronym Dictionary

Term	Meaning
AFWA	U.S. Air Force Weather Agency
AMSL	above mean sea level
APD	avalanche photodiode

Term	Meaning
ASR	attenuated scattering ratio
AU	astronomical unit
BITS	Built In Test System
CALIOP	Cloud-Aerosol Lidar with Orthogonal Polarization
CALIPSO	Cloud-Aerosol Lidar and Infrared Pathfinder Satellite Observation
CERES	Clouds and the Earth's Radiant Energy System
COTS	commercial off-the-shelf
CPL	Cloud Physics Lidar
CVD	Color Vision Deficiency
DAAC	Distributed Active Archive Centers
DEM	digital elevation model
ECEF	Earth-centered, Earth-fixed
ECR	Earth Centered Rotating
EOS	Earth Observing System
FP-IT	Forward Processing – Instrument Teams
frame	a fundamental data averaging interval used extensively in CALIOP's level 1 and level 2 data processing. A frame consists of 15 consecutive single-shot profiles spanning an along-track distance of ~5 km. 15 shots is the least common multiple of the along-track averaging intervals defined by CALIOP's vertically varying onboard data averaging scheme (Hunt et al., 2009).
GEOS-4	Goddard Earth Observing System Model, Version 4
GEOS-5	Goddard Earth Observing System Model, Version 5
GMAO	Global Modeling and Assimilation Office
GOMOS	Global Ozone Monitoring by Occultation of Stars
granule	continuous data segment in which all measurements were acquired while the lidar was configured for daytime data acquisition only or nighttime data acquisition only; each granule spans approximately one half of a full orbit, with daytime granules being slightly larger/longer than nighttime granules
GTOPO30	A global digital elevation model with a horizontal grid spacing of 30 arc seconds
HDF	Hierarchical Data Format
HSRL	high spectral resolution lidar
IGBP	International Geosphere–Biosphere Programme
IIR	imaging infrared radiometer
L1B	level 1B
LEM	low energy mitigation
LOM	laser optics module
LRE	lidar receiver electronics
LSWG	Lidar Science Working Group
MAD	median absolute difference
MERRA-2	Modern-Era Retrospective analysis for Research and Applications, Version 2
MHz	megahertz

Term	Meaning
MLS	Microwave Limb Sounder
MODIS	Moderate Resolution Imaging Spectroradiometer
MSL	mean sea level
N/A	not applicable
NASA	National Aeronautics and Space Administration
NSA	negative signal anomaly
NSF	noise scale factor
NSIDC	National Snow and Ice Data Center
PDAC	Payload Data Acquisition Cycle
PGR	polarization gain ratio
PMT	photomultiplier tube
PSC	polar stratospheric cloud
PSSP	pseudo single shot profiles
QC	quality control
RMS	root mean square
SAA	South Atlantic Anomaly
SAD	Science Ancillary Data
SAGE	Stratospheric Aerosol and Gas Experiment
SDS	scientific data set
SES	Sun-Earth-Satellite
SIT	system integration test
SNR	signal-to-noise ratio
SDS	scientific data set
sr	steradian
TAI	International Atomic Time
UTC	Coordinated Universal Time
WFC	Wide Field-of-view Camera
WRS	Worldwide Reference System

Scientific Data Sets: Measurement Altitudes

This section enumerates all of the SDSs contained in the V5.0 CALIPSO Lidar Level 1B HDF files and provides a brief description of each.

Lidar_Data_Altitudes

Units: km

Format: Float_32

Valid Range: -2.0, 40.0

Description: Altitudes (above mean sea level) that specify the vertical midpoints of the 583 range bins in the profile measurements downlinked from the CALIPSO satellite. This scientific data set (SDS) is only available in the V5.00 data release. In all prior versions, the lidar data altitude array was stored only in the file metadata.

Met_Data_Altitudes

Units: km

Format: Float_32

Valid Range: -2.0, 40.0

Description: Altitudes (above mean sea level) that specify the vertical midpoints at which the 33 element profiles of ancillary meteorological data are reported. This SDS is only available in the V5.00 data release. In all prior versions, the meteorological data altitude array was stored only in the file metadata.

Scientific Data Sets: Time and Position

Profile_Time

Units: TAI seconds

Format: Float_64

Valid Range: 4.203E8, 9.623E8

Description: Laser firing time for each pulse, given in International Atomic Time (TAI) (i.e., in elapsed seconds from January 1, 1993).

Profile_UTC_Time

Units: yymmdd.ffffffff

Format: Float_64

Valid Range: 60428.0, 230701.0

Description: Laser firing time for each pulse, given in Coordinated Universal Time (UTC) and formatted as yymmdd.ffffffff, where yy is a two digit data acquisition year number (06 to 23), mm is a month number (01 to 12), dd is a day number (1 to 31), and ffffffff is the elapsed fraction of the data acquisition day.

Day_Night_Flag

Units: No Units

Format: Int_8

Valid Range: 0, 1

Description: As CALIPSO approaches the terminator, the lidar is automatically reconfigured to adapt to changing lighting conditions that directly impact signal-to-noise (SNR) levels. These changes occur at Sun-Earth-Satellite (SES) angles of 95° (day to night) and 265° (night to day), corresponding to changes in lighting conditions at an altitude of ~24 km above mean sea level. 0 indicates daytime conditions, 1 indicates nighttime.

Profile_ID

Units: No Units

Format: Int_32

Valid Range: 1, 228630

Description: Unique profile identifier generated sequentially in ground processing for each laser pulse. Profile IDs are guaranteed to be unique within each L1B data file but not over multiple files.

Latitude

Units: degrees north

Format: Float_32

Valid Range: -90.0, 90.0

Fill Value: -9999.0

Description: Geodetic latitude of the laser footprint on the Earth's surface.

Longitude

Units: degrees east

Format: Float_32

Valid Range: -180.0, 180.0

Fill Value: -9999.0

Description: Longitude of the laser footprint on the Earth's surface.

Scientific Data Sets: Lidar Operating Mode

Frame_Number

Units: No Units

Format: Int_16

Valid Range: 1, 11

Description: The downlinked CALIOP data is partitioned into "frames", where each frame contains backscatter profiles for all three measurement channels acquired over 15 consecutive laser pulses (i.e., a 5 km along-track data segment). Frame_Number reports the number of the current frame within the sequence of 11 frames contained within a Payload Data Acquisition Cycle (PDAC). A PDAC is the minimum time interval over which each of the three CALIPSO instruments can all collect an integer number of measurements (165 laser pulses, ~55 km along track).

Lidar_Mode

Units: No Units

Format: Int_16

Valid Range: 1, 6

Description: Lidar operations mode, as given in Table 1. For all L1B data, the lidar mode will always be 3, indicating that the lidar is in autonomous data acquisition mode.

Table 1: Interpretation of the lidar operations mode values

Value	Operations Mode
1	Safe
2	Standby
3	autonomous data collection
4	built in test system (BITS)
5	special operations
6	Diagnostic

Lidar_Submode

Units: No Units

Format: Int_16

Valid Range: 1, 25

Description: Lidar operations submode, as given in Table 2. For all Level 1B data, the lidar submode will be 4, indicating that the lidar was operating in its normal configuration.

Table 2: Interpretation of the lidar operations submode values

Value	Operations Submode		Value	Operations Submode
1	safe		14	baseline measurement

Value	Operations Submode		Value	Operations Submode
2	warm-up		15	polarization calibration
3	standby		16	extended background measurement
4	normal		17	boresight alignment
5	BITS profile #1, no background		18	manual boresight operation
6	BITS profile #2, no background		19	boresight search
7	BITS profile #3, no background		20	build on-board baseline profiles
8	BITS profile #4, no background		21	baseline corrected high gain channel
9	BITS profile #1, with background		22	baseline corrected low gain channel
10	BITS profile #2, with background		23	uncorrected high gain channel
11	BITS profile #3, with background		24	uncorrected low gain channel
12	BITS profile #4, with background		25	diagnostic
13	no baseline removal		26–32	unused

Laser_Energy_532

Units: J

Format: Float_32

Typical Range: 0.003...0.135

Description: 532 nm laser energy measured for each laser pulse by a dedicated onboard laser energy monitor.

Laser_Energy_1064

Units: J

Format: Float_32

Typical Range: 0.038...0.12

Description: 1064 nm laser energy measured for each laser pulse by a dedicated onboard laser energy monitor.

Parallel_Amplifier_Gain_532

Perpendicular_Amplifier_Gain_532

Amplifier_Gain_1064

Units: V/V

Format: Float_32

Typical Range @ 532 nm: 26.0...178.0

Typical Range @ 1064 nm: 102.0...195.0

Fill Value: -9999.0

Description: Gain of the high gain amplifier for, respectively, the 532 nm parallel channel, the 532 nm perpendicular channel, and the 1064 nm channel. For all channels, nighttime gains are substantially higher than daytime gains. Figure 1 in Hunt et al., 2009 shows a block diagram of the CALIOP lidar, including all amplifiers and digitizers.

Off_Nadir_Angle

Units: degrees

Format: Float_32

Valid Range: 0.0, 10.0

Fill Value: -9999.0

Description: Angle of the lidar viewing vector relative to nadir pointing; the off-nadir angle was fixed at 0.3 degrees at launch/first-light and permanently changed to 3.0 degrees after November 28, 2007.

There is some jitter in the off-nadir angle. The mean value for the 51, 719, 250 good laser profiles acquired during October 2014 is 2.9827° ± 0.0128°, with minimum and maximum values of, respectively, 2.9348° and 3.0274°. There is also a very small number of granules in which pointing angle experiments are conducted, and during these events the off-nadir angles can be as large as 30° or more. Appendix 1 lists all granules containing off-nadir angles that vary by more than ±0.5° from the nominal values.

Surface_Altitude_Shift

Units: km

Format: Float_32

Valid Range: -0.15, 0.15

Description: Altitude difference between the range bin at nominal mean sea level (MSL) in each downlinked lidar profile and the MSL range bin in the fixed altitude array to which all profile measurements are registered. Altitudes for the downlinked profile are computed based on photon time of flight as a function of the actual spacecraft off-nadir angle, which varies slightly from the commanded spacecraft off-nadir angle. The Surface Altitude Shift parameter reports the difference between apparent MSL in the downlinked profile and the MSL bin in the fixed altitude array.

Number_Bins_Shift

Units: No Units

Format: Int_32

Valid Range: -8, 8

Description: Number of 30-meter altitude bins shifted by the altitude registration algorithm to achieve the best match between apparent MSL in the measured profile and MSL in CALIOP's fixed altitude array. In the altitude registration process, the bin shift required to register the measured data to CALIOP's fixed altitude grid is designated as positive whenever MSL in the measured data is higher than MSL in the fixed altitude grid. Similarly, whenever MSL in the measured data is lower, the bin shift is designated negative. A schematic of the bin shifting geometry is shown in Figure 1. For measured off-nadir angles very near the commanded CALIOP off-nadir angle, the Number of Bins Shifted is approximately equal to round(Surface Altitude Shift / (0.029979 × cos(off-nadir angle))) (units = km) .

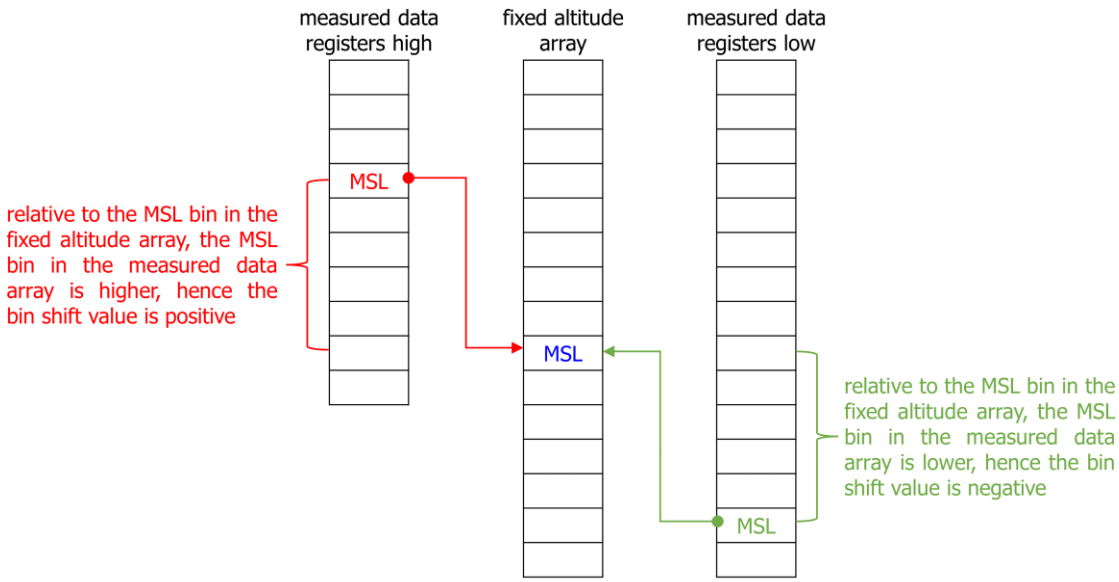

Figure 1. Schematic view of the bin shifting that occurs in the CALIOP altitude registration process.

Scientific Data Sets: Surface Information

Land_Water_Mask

Units: No Units

Format: Int_8

Valid Range: 0, 7

Fill Value: -9

Description: Surface type at the laser footprint obtained from the CloudSat science team digital elevation model (DEM), with values as shown in Table 3.

Table 3: Interpretation of the land-water mask values

Value	Surface Type		Value	Surface Type
0	shallow ocean		4	intermittent water
1	Land		5	deep inland water
2	Coastlines		6	continental ocean
3	shallow inland water		7	deep ocean

IGBP_Surface_Type

Units: No Units

Format: Int_8

Valid Range: 1, 18

Fill Value: -9

Description: International Geosphere–Biosphere Programme (IGBP) surface type at the laser footprint, provided by the CERES Surface Type ID map, with values as shown in Table 4.

Table 4: Interpretation of the IGBP surface type values

Value	Surface Type		Value	Surface Type
1	Evergreen-Needleleaf-Forest		10	Grassland
2	Evergreen-Broadleaf-Forest		11	Wetland
3	Deciduous-Needleleaf-Forest		12	Cropland
4	Deciduous-Broadleaf-Forest		13	Urban
5	Mixed-Forest		14	Crop-Mosaic
6	Closed-Shrubland		15	Permanent-Snow
7	Open-Shrubland (Desert)		16	Barren/Desert
8	Woody-Savanna		17	Water
9	Savanna		18	Tundra

Snow_Ice_Surface_Type

Units: No Units

Format: UInt_8

Valid Range: 0, 255

Description: Snow and ice coverage for the surface at the laser footprint provided by the U.S. Air Force Weather Agency (AFWA). Values between 0 and 100 represent the percentage of ice within a pixel having a nominal resolution of 25 km^2. Pixels with permanent ice are assigned a value of 101. A value of 103 indicates pixels containing snow. 255 indicates mixed type/uncertain type pixels at coastlines. Earlier versions of the CALIOP data products used information obtained from the National Snow and Ice Data Center (NSIDC).

Surface_Elevation

Units: km

Format: Float_32

Valid Range: -1.0, 9.0

Fill Value: -9999.0

Description: Surface elevation at the laser footprint, above local mean sea level (AMSL), obtained from digital elevation model (DEM) developed by the CloudSat science team (Tanelli et al., 2014).

GMAO_Surface_Elevation

Units: km

Format: Float_32

Valid Range: -1.0, 9.0

Fill Value: -9999.0

Description: Surface elevation at the laser footprint (AMSL) used by MERRA-2 to create profiles of meteorological parameters. The spatial resolution of the MERRA-2 DEM is coarser than that of the CloudSat/CALIPSO DEM and thus when large differences between the two estimates are encountered, a remapping routine is employed to ensure consistency between the CALIOP measurements and the MERRA-2 meteorological information.

Scientific Data Sets: Signal Quality

Surface_Saturation_Flag_532Par

Surface_Saturation_Flag_532Perp

Surface_Saturation_Flag_1064

Units: No Units

Format: UInt_8

Valid Range: 0, 2

Description: Reports the likelihood that the surface signal is saturated in, respectively, the 532 nm parallel channel, the 532 nm perpendicular channel, and the 1064 nm channel, with values as listed in Table 5.

Table 5: Interpretation of the surface saturation flag values

Value	Interpretation
0	not saturated
1	possibly saturated
2	certainly saturated

Surface_Saturation_Index_532Par

Surface_Saturation_Index_532Perp

Surface_Saturation_Index_1064

Units: No Units

Format: Int_16

Valid Range: -1, 582

Fill Value: -9999

Description: Reports the zero-based altitude index of the lowest range bin where the surface saturation flag is either "possibly saturated" or "certainly saturated" in, respectively, the 532 nm parallel channel, the 532 nm perpendicular channel, and the 1064 nm channel. For profiles classified as "not saturated" (i.e., saturation flag = 0), a value of -1 is reported.

Negative_Signal_Anomaly_Index_532Par

Negative_Signal_Anomaly_Index_532Perp

Negative_Signal_Anomaly_Index_1064

Units: No Units

Format: Int_16

Valid Range: -1, 582

Fill Value: -9999

Description: A negative signal anomaly (NSA) is identified whenever the L1B attenuated backscatter coefficients show anomalously negative excursions in range bins immediately preceding a strongly scattering target such as the Earth's surface or a dense water cloud. Figure 2 shows an example. This SDS reports the zero-based altitude index of the lowest range bin where an NSA is detected in, respectively, the 532 nm parallel channel, the 532 nm perpendicular channel, and the 1064 nm channel. Profiles in which a negative signal anomaly is not detected report a value of -1.

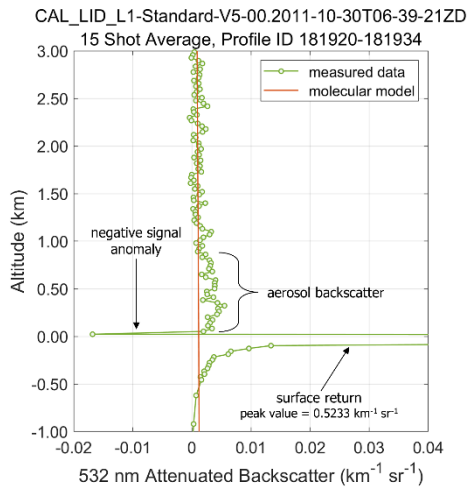

Figure 2: 15 shot (5 km) average of 532 nm total attenuated backscatter profiles measured on 30 October 2011. In this example, NSAs occur repeatedly in the single shot profiles for both the parallel and perpendicular channels.

Parallel_Background_Monitor_532

Perpendicular_Background_Monitor_532

Units: count

Format: Float_32

Typical Range: 120.0...6000.0

Description: Magnitudes of the background signals, in science digitizer counts, for, respectively, the 532 nm parallel and 532 nm perpendicular channels. Background signals are measured for each laser pulse at very high altitudes (112–97 km; see Hunt et al., 2009), where laser backscatter from atmospheric constituents is essentially zero. Background signals include such things as detector dark current and background radiation signals (e.g., from daytime sunlight). CALIPSO lidar signals measured between 40.0 km and the Earth's surface will typically include both an atmospheric backscatter component and a background contribution, although laser backscatter is not measured below opaque features. Background signals are measured and subtracted during the onboard data processing prior to data downlink. Table 6 lists altitude regions, relative to MSL, for all vertically resolved CALIOP measurements.

Table 6: CALIOP data acquisition regions in terms of altitude above MSL. The satellite altitude varies as a function of orbital position, as does the distance between the satellite and the data digitization start. The data digitization start altitude is fixed, as are all altitudes below.

Region Number	Altitude Range	Nominal Region Name
N/A	705 km – 733 km	Satellite Altitude (varies with latitude)
N/A	120 km	Data Digitization Start (fixed)
N/A	112 km to 97 km	Background Monitor Measurement Region
6	80 km to 65 km	High Altitude RMS Baseline Measurement Region
5	40.0 km to 30.1 km	Mid-Stratosphere
4	30.1 km to 20.2 km	Lower Stratosphere
3	20.2 km to 8.2 km	Upper Troposphere
2	8.2 km to –0.5 km	Lower Troposphere

Region Number	Altitude Range	Nominal Region Name
1	–0.5 km to –2.0 km	Subsurface
0	–11.0 km to –18.0 km	Deep Subsurface RMS Baseline Measurement Region

Parallel_RMS_Baseline_532

Perpendicular_RMS_Baseline_532

RMS_Baseline_1064

Units: count

Format: Float_32

Typical Range: 0.0...3200.0

Description: Root mean square (RMS), in science digitizer counts, of the high-altitude signal measured onboard for each laser pulse over 1000 15 m samples acquired in the 65-80 km baseline altitude range in, respectively, the 532 nm parallel and perpendicular channels and the 1064 nm channel (Hunt et al., 2009). Since atmospheric backscatter is negligible within this region, the squared RMS baseline values provide a scaled measure of the background noise in each profile. Figure 3 illustrates the relationship between these two quantities for all single shot daytime measurements acquired on 5 February 2014.

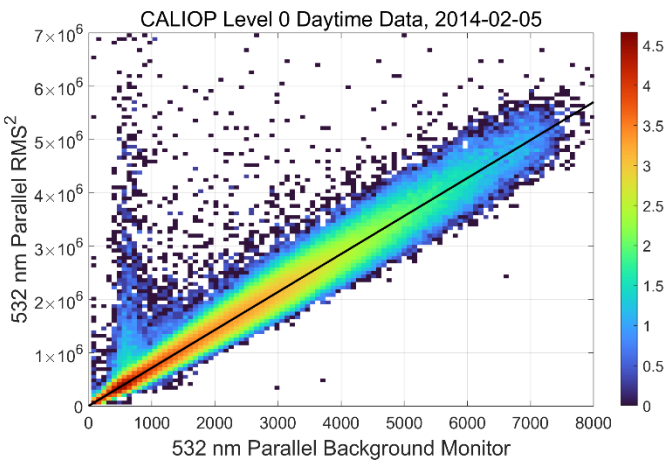

Figure 3: Square of the single shot RMS baseline measurements versus the background monitor readings for all daytime data acquired on 5 February 2014. The solid black line shows a linear least squares fit, $Y = C_0 + C_1 \cdot X$, with $C_0 = 0.008308\times10^6$ and $C_1 = 711.5248$.

Scientific Data Sets: Calibration Coefficients

Calibration_Constant_532

Units: (km^3 * sr * count)/J

Format: Float_32

Typical Range: 3.0E10...8.0E10

Description: The lidar calibration coefficient for the 532 nm parallel channel computed and reported for each single shot backscatter profile. The CALIPSO V5.0 532 nm calibration algorithms are for the most part identical to the V4.1 algorithms presented in Kar et al., 2018 (nighttime calibration) and Getzewich et al., 2018 (daytime calibration). The sole change of note is that the daytime calibration procedure was updated to mitigate the impact of low energy pulses that started occurring late in 2016, prevailingly in the South Atlantic Anomaly (SAA) region (Noel et al., 2014; Tackett et al., 2025).

For nighttime orbit segments, the 532 nm calibration constants are derived by comparing the 532 nm parallel channel signals measured between 36 km and 39 km to an attenuated backscatter model derived from molecular and ozone number densities provided by the MERRA-2 reanalysis product produced by NASA's Global Modeling and Assimilation Office. As described in Kar et al., 2018, individual samples are estimated using data averaged over 55 km (165 laser pulses) along track. Samples containing large radiation-induced outliers are rejected by an in-line noise filter. This filter also efficiently rejects low energy laser pulses. Composite calibration coefficients for each profile within a nighttime granule are then calculated using a two-dimensional moving average. A schematic of this averaging scheme is shown in the figure below. In this example, calibration constants for each profile along the central orbit track, shown in yellow, are computed by averaging all 55 km samples within a 605 km sliding window (red rectangles, not to scale) that extends ±5 granules about the granule being calibrated.

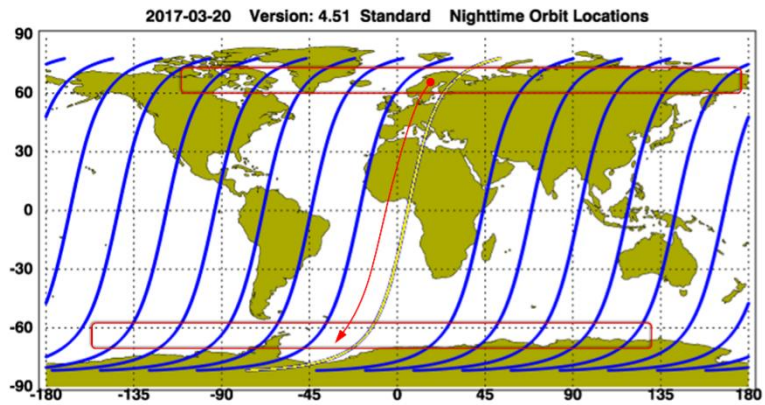

Figure 4: Graphic representation of the two-dimensional averaging scheme used to harvest CALIOP's nighttime calibration coefficients. CALIPSO nighttime orbit tracks for March 20, 2017 are shown in blue. The red arrow in the center indicates the satellite direction of travel. The red boxes at the top and bottom of the image span 11 consecutive orbits, with the midpoint ground track shown in yellow. The vertical span of the red boxes (not to scale) is 605 km (1815 consecutive laser pulses). Calibration coefficients for the central orbit track (in yellow) are computed using a running average of all data enclosed by the red box, starting at the day-to-night terminator in the Arctic and ending at the night-to-day terminator over Antarctica.

The 532 nm molecular backscatter in the perpendicular channel is far too faint to be used successfully in the molecular normalization technique used for the parallel channel. Instead, the perpendicular channel calibration coefficient is derived by dividing the parallel channel calibration coefficient by the depolarization gain ratio described below.

The calibration technique used during the nighttime cannot be used in the daytime portions of the orbits because the noise associated with solar background signals (i.e., sunlight) degrades the backscatter SNR in the 36-39 km calibration region far below usable levels. To obtain acceptable SNR, 532 nm daytime parallel channel calibration constants are derived by matching the attenuated scattering ratios measured during the daytime in the lower stratosphere (e.g., ~20-24 km in the tropics) to the attenuated scattering ratios measured in the same altitude region during nighttime orbit segments, where the signals have already been calibrated. As explained in Getzewich et al., 2018, this procedure assumes that the aerosol loading in the daytime calibration regions remains diurnally invariant over the averaging intervals required to obtain acceptable calibration SNR. Obtaining daytime calibration SNR commensurate with nighttime values requires averaging daytime signals over 105 consecutive orbits.

Calibration_Constant_Uncertainty_532

Units: (km^3 * sr * count)/J

Format: Float_32

Typical Range: 2.0E8...1.6E9

Description: Estimated uncertainty due to random noise in the 532 nm calibration coefficients, computed and reported for each single shot profile. For nighttime calibrations, the mean uncertainty due to noise is estimated to be 1.6% ± 2.4% (Kar et al., 2018). Because the daytime calibration constants are interpolated from nighttime values, the daytime calibrations inherit uncertainties from the nighttime calibrations. In general, and for equal averaging intervals, the uncertainties for daytime calibration coefficients are somewhat higher than for nighttime coefficients. Additional systematic errors, which are not included in the calibration uncertainty estimates, may arise from aerosol contamination within the calibration region (typically well less than a 1–2%), and/or from large signal spikes seen frequently in the SAA and occasionally elsewhere. The CALIOP daytime and nighttime calibration coefficients have been thoroughly validated using multiple underflights by the Langley Research Center (LaRC) high spectral resolution lidars (HSRLs).

Calibration_Constant_1064

Units: (km^3 * sr * count)/J

Format: Float_32

Typical Range: 4.0E9...1.0E10

Description: Calibration constant at 1064 nm reported for each single shot profile. The molecular normalization procedure used to calibrate the 532 nm signals cannot be applied for the 1064 nm measurements, because the molecular scattering at 1064 nm is ~17 times weaker than at 532 nm, and because the avalanche photodiode (APD) detector used in the 1064 nm channel has significantly higher dark noise than the 532 nm photomultiplier tubes (PMTs). To circumvent these difficulties, CALIOP's 1064 nm channel is calibrated relative to the 532 nm channel using the backscatter from a carefully selected subset of ice cloud measurements (Vaughan et al., 2019). Candidate clouds contaminated by low energy laser pulses are excluded (Tackett et al., 2025). Unlike the 532 nm calibrations, at 1064 nm the same procedure is used for both daytime and nighttime calibrations.

Calibration_Constant_Uncertainty_1064

Units: (km^3 * sr * count)/J

Format: Float_32

Typical Range: 5.0E7...4.0E9

Description: Estimated uncertainty in the 1064 nm calibration constant, computed and reported for each single shot profile. Unlike the 532 nm calibration constant uncertainties, the uncertainties reported for the 1064 nm calibration constants include contributions from both random errors, which can be reduced by averaging, and systematic biases, which cannot be reduced by averaging. Systematic biases arise from biases in the 532 nm calibration constants and the assumption of a fixed backscatter color ratio for cirrus clouds (i.e., β_{1064}/β_{532} = 1.01). Random errors are introduced by the SNRs at both 532 nm and 1064 nm within the cirrus clouds used in the calibration routine. A full accounting of 1064 nm calibration constant uncertainties in given in section 4.3 of Vaughan et al., 2019.

Depolarization_Gain_Ratio_532

Units: No Units

Format: Float_32

Typical Range: 0.0...2.5

Fill Value: -9999.0

Description: The (de)polarization gain ratio (PGR) is an essential calibration coefficient that quantifies the ratio of the opto-electric gains in the 532 nm perpendicular and parallel channels. The 532 nm nighttime PGR is calculated from routine PGR calibration operations in which a pseudo-depolarizer is inserted into the receiver optical path to generate equal backscatter intensities in both 532 nm channels. The 532 nm daytime PGR is derived from the perpendicular and parallel channel RMS baseline measurements acquired above optically thick ice clouds. The PGR is a required parameter for calibrating the perpendicular channel

attenuated backscatter coefficients. Given the PGR and the parallel channel calibration coefficient, $C_{\parallel}$, the perpendicular channel calibration coefficient, $C_{\perp}$, is calculated using $C_{\perp} = C_{\parallel}$ / PGR.

Depolarization_Gain_Ratio_Uncertainty_532

Units: No Units

Format: Float_32

Typical Range: 0.0...0.01

Fill Value: -9999.0

Description: Absolute uncertainty in the 532 nm depolarization gain ratio (PGR) due to random noise. The mean relative uncertainty for nighttime PGRs measured over the full mission is 0.22% ± 0.07%. While systematic errors are not included, they are estimated to be similarly small.

Scientific Data Sets: Backscatter Profiles

Total_Attenuated_Backscatter_532

Units: 1/(km * sr)

Format: Float_32

Typical Range: -0.1...3.3

Fill Value: -9999.0

Description: Profiles of total attenuated backscatter coefficients at 532 nm, $\beta'_{532}(z)$, are arguably CALIOP's primary level 1 data product. At any altitude $\beta'_{532}(z)$ is both (a) the product of the height-dependent 532 nm volume backscatter coefficient and the two-way transmittance (signal attenuation) from the lidar to the sample volume, and (b) the sum of the attenuated backscatter coefficients measured in the 532 nm parallel and perpendicular channels. The parallel and perpendicular channel attenuated backscatter coefficients are derived from the calibrated, range-corrected, gain and laser energy normalized, background and baseline subtracted lidar return signals. The CALIOP data products report total and perpendicular channel attenuated backscatter coefficients. Parallel channel values are derived by subtracting the perpendicular contribution from the total. 532 nm volume depolarization ratios can then be obtained by dividing the perpendicular attenuated backscatter coefficients by the parallel.

While $\beta'_{532}(z)$ are reported for each laser pulse as an array of 583 elements that have been registered to a constant altitude grid defined by the Lidar_Data_Altitudes field, the spatial resolution of each range bin is not uniform throughout. To meet hardware constraints imposed on downlink data volume, CALIOP profiles are averaged onboard the satellite prior to being transmitted to the ground station. As shown in the table below, different horizontal and vertical resolutions are defined for different altitude regimes, with greater amounts of averaging done at higher altitudes where the atmosphere is expected to be more homogeneous.

Table 7: CALIOP's onboard data averaging scheme. Profile data are sampled onboard at 10 MHz (~15 m vertical resolution) then averaged to the spatial resolutions shown below prior to being downlinked. The number of bins given in the Vertical Resolution columns specifies the number of ~15 m bins averaged onboard to create a single vertical sample prior to downlink.

Region	Nominal Altitude Range (km)	Bin Numbers	Horizonal Resolution	532 nm Vertical Resolution	1064 nm Vertical Resolution
5	40.0 – 30.1	1 – 33	15 laser pulses (5 km)	20 bins (300 m)	N/A
4	30.1 – 20.2	34 – 88	5 laser pulses (5/3 km)	12 bins (180 m)	12 bins (180 m)
3	20.2 – 8.3	89 – 288	3 laser pulses (1 km)	4 bins (60 m)	4 bins (60 m)
2	8.3 – -0.5	289 – 578	1 laser pulse (1/3 km)	2 bins (30 m)	4 bins (60 m)

Region	Nominal Altitude Range (km)	Bin Numbers	Horizonal Resolution	532 nm Vertical Resolution	1064 nm Vertical Resolution
1	-0.5 – -2.0	578 – 583	1 laser pulse (1/3 km)	20 bins (300 m)	20 bins (300 m)

Profiles of attenuated backscatter coefficient uncertainties are not explicitly reported in the CALIOP L1B products, as doing so would approximately double the (already large) file sizes. Instead, users can compute random error estimates for the attenuated backscatter products using various parameters reported in the L1B files (e.g., noise scale factors and RMS baseline measurements) and the procedure outlined in Appendix 2 at the end of this document.

Perpendicular_Attenuated_Backscatter_532

Units: 1/(km * sr)

Format: Float_32

Typical Range: -0.08...1.7

Fill Value: -9999.0

Description: Perpendicular channel component of the 532 nm total attenuated backscatter coefficients and reported in the same format. Profiles of the parallel channel component of the 532 nm total attenuated backscatter coefficients can be obtained by subtracting the perpendicular from the total.

Attenuated_Backscatter_1064

Units: 1/(km * sr)

Format: Float_32

Typical Range: -0.04...2.5

Fill Value: -9999.0

Description: Attenuated backscatter coefficients at 1064 nm, $\beta'_{1064}(z)$, derived from the calibrated, range-corrected, gain and laser energy normalized, background and baseline subtracted lidar return signal. The magnitude of the 1064 nm molecular attenuated backscatter is a ~17 times lower than the 532 nm molecular attenuated backscatter, and hence (absent a huge volcanic eruption or a renegade PSC) there is no useable 1064 nm signal in the 30.1 - 40 km altitude range. Consequently, the first 33 bins of each profile contain fill values. Otherwise, the format of the 1064 nm attenuated backscatter SDS is wholly identical to the format of the 532 nm attenuated backscatter SDS.

Noise_Scale_Factor_532_Parallel

Noise_Scale_Factor_532_Perpendicular

Units: count^(1/2)

Format: Float_32

Typical Parallel Channel Range: 4.0...8.0

Typical Perpendicular Channel Range: 3.4...8.0

Description: The noise scale factor (NSF) is a calculated constant of proportionality that quantifies the relationship between the root mean square of the random noise in a measurement and the square root of the mean signal being measured. As an example, for Poisson-distributed noise, where the mean and variance are equal, the NSF is one. This SDS reports the NSF for each laser 532 nm pulse, computed from daytime measurements of the RMS Baseline 532 and Background Monitor 532 readings for, respectively, the 532 nm parallel and 532 nm perpendicular channel. Guidance on using the noise scale factors to estimate random uncertainties in the CALIOP attenuated backscatter coefficients is given below in Appendix 2.

Noise_Scale_Factor_1064

Units: count^(1/2)

Format: Float_32

Typical Range: 0.0

Description: CALIOP does not measure the background signal level at 1064 nm, because the APD detector dark noise is dominant during both nighttime and daytime measurement. For this reason, the procedure to estimate the NSF for the 532 nm channels cannot be used for the 1064 nm channel. Consequently, the 1064 nm NSF reported in this SDS is always set to 0. This causes negligible error because, as above, the APD detector dark noise is the dominant error source.

Scientific Data Sets: Reflectances

Parallel_Column_Reflectance_532

Perpendicular_Column_Reflectance_532

Units: No Units

Format: Float_32

Typical Range: 0.0...1.0

Fill Value: -9999.0

Description: Bi-directional column reflectances derived from the depolarization gain ratio and, respectively, the parallel and perpendicular RMS baseline measurements at 532 nm.

Parallel_Column_Reflectance_Uncertainty_532

Perpendicular_Column_Reflectance_Uncertainty_532

Units: No Units

Format: Float_32

Typical Range: 0.0...0.45

Fill Value: -9999.0

Description: Column reflectance uncertainties derived for, respectively, the 532 nm parallel channel and the 532 nm perpendicular channel.

Reflectance_Calibration_Coefficient_532

Units: (W * 1/m^2 * 1/sr) / counts

Format: Float_32

Typical Range: 4.9e-05...7.5e-05

Fill Value: -9999.0

Description: Calibration coefficient used in converting the sum of the squares of the RMS baseline measurements (units = CALIOP science digitizer counts) to radiances (units = $W \times m^{-2} \times sr^{-1}$).

Reflectance_Calibration_Coefficient_Uncertainty_532

Units: (W * 1/m^2 * 1/sr) / counts

Format: Float_32

Typical Range: 2.2e-06...3.8e-06

Fill Value: -9999.0

Description: Absolute uncertainty in the calibration coefficients that convert the sum of the squares of the RMS baseline measurements to radiances.

Scientific Data Sets: Ancillary Meteorological Data

Molecular_Number_Density

Units: molecules/m^3

Format: Float_32

Valid Range: 4.8E22, 4.8E25

Description: Molecular number density reported for each lidar Level 1 profile at the 33 standard altitudes recorded in the Met Data Altitudes field. Molecular number density profiles are obtained from the MERRA-2 ancillary meteorological data.

Ozone_Number_Density

Units: molecules/m^3

Format: Float_32

Valid Range: 9.0E16, 1.0E19

Description: Ozone number density reported for each lidar Level 1 profile at the 33 standard altitudes recorded in the Met Data Altitudes field. Ozone number density profiles are obtained from the MERRA-2 ancillary meteorological data.

Temperature

Units: °C

Format: Float_32

Valid Range: -120.0, 60.0

Description: Temperature reported for each lidar Level 1 profile at the 33 standard altitudes recorded in the Met Data Altitudes field. Temperature profiles are interpolated from the MERRA-2 ancillary meteorological data.

Pressure

Units: hPa

Format: Float_32

Valid Range: 1.0, 1086.0

Description: Pressure reported for each lidar Level 1 profile at the 33 standard altitudes recorded in the Met Data Altitudes field. Pressure profiles are interpolated from the MERRA-2 ancillary meteorological data.

Relative_Humidity

Units: %

Format: Float_32

Valid Range: 0.0, 150.0

Description: Relative humidity reported for each lidar Level 1 profile at the 33 standard altitudes recorded in the Met Data Altitudes field. Relative humidity profiles are interpolated from the MERRA-2 ancillary meteorological data.

Surface_Wind_Speeds_02m

Surface_Wind_Speeds_10m

Units: m/s

Format: Float_32

Valid Range: -80.0, 80.0

Description: Surface wind speeds at, respectively, 2 m and 10 m above the Earth's surface. Wind speeds are interpolated from the MERRA-2 ancillary meteorological data and reported for each laser pulse as N × 2 arrays, where the first column gives the magnitude of the eastward, zonal, u component and the second column reports the northward, meridional, v component.

Tropopause_Height

Units: km

Format: Float_32

Valid Range: 4.0, 22.0

Description: Tropopause heights AMSL interpolated from the MERRA-2 ancillary meteorological data and reported for each lidar Level 1 profile.

Tropopause_Temperature

Units: °C

Format: Float_32

Valid Range: -95.0, -20.0

Description: Tropopause temperatures, interpolated from the MERRA-2 ancillary meteorological data and reported for each lidar Level 1 profile.

Scientific Data Sets: Quality Assurance

QC_Flag

Units: No Units

Format: UInt_32

Valid Range: 0, 16777215

Description: CALIOP level 1 quality control (QC) flags are unsigned 32-bit integers, with each bit indicating a specific error condition, as defined Table 8. Prior to being downlinked, CALIPSO lidar data are averaged on-board the satellite using the variable averaging scheme shown in Table 1. Regions 1 and 2 contain single shot data (albeit at different vertical resolutions). In regions 3, 4, and 5, the downlinked data have been averaged to horizontal resolutions of, respectively, 3 shots, 5 shots, and 15 shots. The level 1 processing constructs pseudo single shot profiles (PSSP) by replicating the data from regions 3, 4, and 5, and then stacking the data arrays from the different averaging regions. Two sets of QC flags, as defined in Table 8 and Table 9, are computed for each one of these pseudo single shot profiles.

The laser energy assessments reported in the QC flag are interpreted as follows:

- the laser energies evaluated by bits 5, 6, 13, and 14 correspond to the energies for the pure single shot portion of each PSSP (i.e., from altitude regions 1 and 2 only);
- bits 15-19 are toggled on if any single shot within the horizontally averaged regions of a PSSP falls below the 'near zero energy' threshold (i.e., $E_{532} < 0.01$ J, $E_{1064} < 0.0408$ J); and
- bits 20-24 are toggled on if any single shot within the horizontally averaged regions of a PSSP falls below the 'data quality' threshold (i.e., $E_{532} < 0.05$ J, $E_{1064} < 0.05$ J).

For example, suppose that the energies for shot #5 in a 15-shot frame fail the data quality threshold tests but are above the 'near zero' thresholds; and (b) the energies for all other shots in the frame are normal. In this case, bits 5, 6, 13, and 14 in profiles 1-4 and 6-15 are all set to zero, to indicate acceptable laser energy. In profile #5, bits 5 and 6 are zero (because the energies were above the 'near zero' threshold) and bits 13 and 14 are one (because the energies were below the data quality threshold). Because the averaged data in region 3 of PSSP #4, #5, and #6 was constructed using the low energy data recorded for shot #5, bits 15 and 16 in these three profiles are set to one, whereas in the remaining profiles bits 15 and 16 are

set to zero. Similarly, bits 17 and 18 are set to one for PSSP #1 - #5, and bit 19 is set to one for all profiles in the 15-shot frame.

Table 8: Interpretation of the bits in the CALIOP QC flag; region altitudes are given in Table 6

Bit(s)	Interpretation
1	532 nm parallel channel missing
2	532 nm perpendicular channel missing
3	1064 nm channel missing
4	Not geolocated
5	Single shot 532 laser energy below calibration threshold (< 0.01 J; near zero energy)
6	Single shot 1064 laser energy below calibration threshold (< 0.0408 J; near zero energy)
7	Historical value used for the depolarization gain ratio
8	Historical calibration constant used, 532 nm parallel channel
9	Historical calibration constant used, 532 nm perpendicular channel
10	Historical calibration constant used, 1064 nm channel
11	Averaged calibration constant used, 532 nm parallel channel
12	Averaged calibration constant used, 532 nm perpendicular channel
13	Single shot 532 laser energy below data quality threshold (< 0.05 J; low energy)
14	Single shot 1064 laser energy below data quality threshold (< 0.05 J; low energy)
15	Near zero 532 nm laser energy profile included in region 3 average
16	Near zero 1064 nm laser energy profile included in region 3 average
17	Near zero 532 nm laser energy profile included in region 4 average
18	Near zero 1064 nm laser energy profile included in region 4 average
19	Near zero 532 nm laser energy profile included in region 5 average
20	Low 532 nm laser energy profile included in region 3 average
21	Low 1064 nm laser energy profile included in region 3 average
22	Low 532 nm laser energy profile included in region 4 average
23	Low 532 nm laser energy profile included in region 4 average
24	Low 532 nm laser energy profile included in region 5 average
25–32	Spare

QC_Flag_2

Units: No Units

Format: UInt_32

Valid Range: 0, 134217727

Description: Quality control flag #2, with individual bits interpreted shown in Table 9.

Table 9: Interpretation of the bits in the CALIOP QC flag 2. Region 6 is the high-altitude RMS baseline measurement region between 80 km and 65 km. Region 2 is the lower tropopause science data acquisition region between 8.2 km and –0.5 km.

Bit(s)	Interpretation
1	Reserve
2	Excessive digitizer underflows, 532 nm parallel channel in region 6
3	Excessive digitizer underflows, 532 nm perpendicular parallel channel, region 6
4	Excessive digitizer underflows, 1064 nm channel, region 6
5	Excessive digitizer overflows, 532 nm parallel channel, region 6
6	Excessive digitizer overflows, 532 nm perpendicular parallel channel, region 6
7	Excessive digitizer overflows, 1064 nm channel, region 6
8	Excessive digitizer overflows, 532 nm parallel channel, region 2
9	Excessive digitizer overflows, 532 nm perpendicular parallel channel, region 2
10	Excessive digitizer overflows, 1064 nm channel, region 2
11	LRE Flags in SAD packet indicate bad data, 532 nm parallel channel
12	LRE Flags in SAD packet indicate bad data, 532 nm perpendicular channel
13	LRE Flags in SAD packet indicate bad data, 1064 nm channel
14	Quality Flags in SAD packet indicate bad data, 532 nm parallel channel
15	Quality Flags in SAD packet indicate bad data, 532 nm perpendicular channel
16	Quality Flags in SAD packet indicate bad data, 1064 nm channel
17	Suspicious offset calculation, 532 nm parallel channel
18	Suspicious offset calculation, 532 nm perpendicular channel
19	Suspicious offset calculation, 1064 nm channel
20	Suspicious mean signal value, 532 nm parallel channel (any/all regions)
21	Suspicious mean signal value, 532 nm perpendicular channel (any/all regions)
22	Suspicious mean signal value, 1064 nm channel (any/all regions)
23	RMS baseline noise out of range, 532 nm parallel channel
24	RMS baseline noise out of range, 532 nm perpendicular parallel channel
25	RMS baseline noise out of range, 1064 nm channel
26	Near surface meteorological parameters were remapped to DEM surface altitude
27	1064 nm calibration coefficients suspect due to low temperatures associated with LRE power up (Vaughan et al., 2019)
28–32	Spare

Scientific Data Sets: Orbital Environment

Viewing_Zenith_Angle

Units: degrees

Format: Float_32

Valid Range: 0.0, 90.0

Fill Value: -9999.0

Description: Angle between the lidar viewing vector and the zenith vector at the lidar footprint on the surface.

Viewing_Azimuth_Angle

Units: degrees

Format: Float_32

Valid Range: -180.0, 180.0

Fill Value: -9999.0

Description: Azimuth angle from north of the lidar viewing vector.

Solar_Zenith_Angle

Units: degrees

Format: Float_32

Valid Range: 0.0, 180.0

Fill Value: -9999.0

Description: Angle between the zenith vector at the lidar footprint on the surface and the line of sight to the sun.

Solar_Azimuth_Angle

Units: degrees

Format: Float_32

Valid Range: -180.0, 180.0

Fill Value: -9999.0

Description: Azimuth angle from north of the line of sight to the sun.

Scattering_Angle

Units: degrees

Format: degrees

Valid Range: 0.0, 180.0

Fill Value: -9999.0

Description: Angle between the lidar viewing angle and the line of sight of the sun.

Scientific Data Sets: Spacecraft Position and Attitude

Spacecraft_Altitude

Units: km

Format: Float_32

Valid Range: 700.0, 740.0

Fill Value: -9999.0

Description: Satellite altitude above mean sea level.

Spacecraft_Position

Units: km

Format: Float_64

Valid Range: -8000.0, 8000.0

Fill Value: -9999.0

Description: Position of the CALIPSO satellite expressed in Earth Centered Rotating (ECR) coordinates (also known as Earth-centered, Earth-fixed (ECEF) coordinates).

Spacecraft_Velocity

Units: km/s

Format: Float_64

Valid Range: -10.0, 10.0

Fill Value: -9999.0

Description: Velocity (ECEF coordinates) of the satellite.

Spacecraft_Attitude

Units: degrees

Format: Float_64

Valid Range: -180.0, 180.0

Fill Value: -9999.0

Description: Attitude (roll, pitch, yaw) of the satellite.

Spacecraft_Attitude_Rate

Units: degrees/s

Format: Float_64

Valid Range: -10.0, 10.0

Fill Value: -9999.0

Description: Rate of change of the satellite attitude.

Subsatellite_Latitude

Units: degrees

Format: Float_32

Valid Range: -90.0, 90.0

Fill Value: -9999.0

Description: Latitude of the geodetic subsolar point, which is the point on the surface where the geodetic zenith vector points toward the satellite.

Subsatellite_Longitude

Units: degrees

Format: Float_32

Valid Range: -180.0, 180.0

Fill Value: -9999.0

Description: Longitude of the geodetic subsolar point, which is the point on the surface where the geodetic zenith vector points toward the satellite.

Earth_Sun_Distance

Units: AU

Format: Float_64

Valid Range: 0.98, 1.02

Fill Value: -9999.0

Description: The distance to the Sun from the Earth's surface at the laser footprint.

Subsolar_Latitude

Units: degrees

Format: Float_32

Valid Range: -90.0, 90.0

Fill Value: -9999.0

Description: Latitude of the geodetic subsolar point, which is the point on the surface where the geodetic zenith vector points toward the Sun.

Subsolar_Longitude

Units: degrees

Format: Float_32

Valid Range: -180.0, 180.0

Fill Value: -9999.0

Description: Longitude of the geodetic subsolar point, which is the point on the surface where the geodetic zenith vector points toward the Sun.

Metadata Parameters

Product_ID

An 80-byte character string that reports the data product name. For the lidar level 1B data, this parameter is "L1_Lidar_Science".

Date_Time_at_Granule_Start

A 27-byte character string that specifies the granule UTC start date and time. The format is yyyy-mm-ddThh:nn:ss.ffffffZ, where yyyy is the year, mm is the month, dd is the day, hh is the hour, nn is the minute, ss is the second, and ffffff is the fractional second. Date and time are separated by the character 'T'. The 'Z' indicates that time is given in UTC.

Date_Time_at_Granule_End

A 27-byte character string that specifies the granule UTC end date and time. The format is yyyy-mm-ddThh:nn:ss.ffffffZ, where yyyy is the year, mm is the month, dd is the day, hh is the hour, nn is the minute, ss is the second, and ffffff is the fractional second. Date and time are separated by the character 'T'. The 'Z' indicates that time is given in UTC.

Date_Time_at_Granule_Production

A 27-byte character string that specifies the UTC date and time at which the level 1b data file was generated. The format is yyyy-mm-ddThh:nn:ss.ffffffZ, where yyyy is the year, mm is the month, dd is the day, hh is the hour, nn is the minute, ss is the second, and ffffff is the fractional second. Date and time are separated by the character 'T'. The 'Z' indicates that time is given in UTC.

Number_of_Bad_Profiles

A 32-bit integer specifying the number of bad attenuated backscatter profiles contained in the granule. Profiles are considered bad if (a) any of the three measurement channels are missing (see bits 0, 1, and 2 in the QC Flags SDS); (b) the measurement data could not be geolocated (see bit 3 in the QC flags SDA); or (c) the energy in either the 532 nm or 1064 nm channel falls below the low energy threshold (see bits 5 and 6 in the QC Flags SDS).

Number_of_Good_Profiles

A 32-bit integer specifying the number of good (i.e., not identified as being bad) attenuated backscatter profiles contained in the granule.

Initial_Subsatellite_Latitude

This field reports the first subsatellite latitude of the granule.

Initial_Subsatellite_Longitude

This field reports the first subsatellite longitude of the granule.

Final_Subsatellite_Latitude

This field reports the last subsatellite latitude of the granule.

Final_Subsatellite_Longitude

This field reports the last subsatellite longitude of the granule.

Orbit_Number_at_Granule_Start

Orbit_Number_at_Granule_End

Orbit_Number_Change_Time

Orbit Number consists of three fields that define the number of revolutions by the CALIPSO spacecraft around the Earth. This number is incremented each time the spacecraft passes the equator on the ascending node. To maintain consistency between the CALIPSO and CloudSat orbit parameters, the Orbit Number is keyed to the CloudSat orbit 2121 at 23:00:47 on 2006/09/20. Because the CALIPSO data granules are organized according to satellite lighting conditions, based on fixed Sun-Earth-Satellite angles, day/night boundaries do not coincide with transition points for defining orbit number. As such, three parameters are needed to describe the orbit number for each granule as:

- **Orbit Number at Granule Start:** orbit number at the granule start time.
- **Orbit Number at Granule End:** orbit number at the granule stop time.
- **Orbit Number Change Time:** time at which the orbit number changes in the granule.

Path_Number_at_Granule_Start

Path_Number_at_Granule_End

Path_Number_Change_Time

Path Number consists of three fields that define an index ranging from 1-233 that references orbits to the Worldwide Reference System (WRS). This global grid system was developed to support scene identification for LandSat imagery. Since the A-Train is maintained to the WRS grid within ±10 km, the Path Number provides a convenient index to support data searches, instead of having to define complex latitude and longitude regions along the orbit track. The Path Number is incremented after the maximum latitude in the orbit is attained and changes by a value of 16 between successive orbits. Because the CALIPSO data granules are organized according to satellite lighting conditions, based on fixed Sun-Earth-Satellite angles, day/night boundaries do not coincide with transition points for defining path number. As such, three parameters are needed to describe the path number for each granule as:

- **Path Number at Granule Start:** path number at the granule start time.
- **Path Number at Granule End:** path number at the granule stop time.
- **Path Number Change Time:** time at which the path number changes in the granule.

While CALIPSO was formation flying in the A-Train all path numbers are exact. Beginning in September 2018, when CALIPSO lowered its orbit into the C-Train, path numbers are no longer exact, but instead indicate the closest WRS reference orbit.

Ephemeris_Files_Used

This 160-byte character field reports a maximum of two ephemeris files used in post-processing of the spacecraft position and velocity fields.

Attitude_Files_Used

This 160-byte character field reports a maximum of two attitude files used in post-processing of the spacecraft attitude and attitude rate fields.

GMAO_Files_Used

This 160-byte character field reports the MERRA-2 data products provided by the GMAO used in processing.

Snow_Ice_Files_Used

This 160-byte character field reports the NSIDC data products provided by NSIDC and reformatted by CERES used in processing.

GEOS_Version

This 64-byte character field reports the version of the MERRA-2 data product provided by the GMAO.

Percent_532-parallel_Bad

Percent_532-perpendicular_Bad

Percent_1064_Bad

These fields report the percentage of bad attenuated backscatter profiles contained in the granule for, respectively, the 532 nm parallel channel, the 532 nm perpendicular channel, and the 1064 nm channel.

Percent_532-parallel_Missing

Percent_532-perpendicular_Missing

Percent_1064_Missing

These fields report the percentage of missing attenuated backscatter profiles in the granule for, respectively, the 532 nm parallel channel, the 532 nm perpendicular channel, and the 1064 nm channel.

Cal_Region_Top_Altitude_532

This field reports the top altitude of the 532 nm nighttime calibration region. The 532 nm calibration region is fixed between 39 km and 36 km for all nighttime calibrations. The 532 nm daytime calibration transfer region varies as a function of the local 400K potential temperature isotherm (Getzewich et al., 2018), and hence is not suitable for reporting in the file metadata.

Cal_Region_Base_Altitude_532

This field reports the base altitude of the 532 nm nighttime calibration region.

Lidar_Data_Altitudes

Altitudes (above mean sea level) that specify the vertical midpoints of the 583 range bins in the profile measurements downlinked from the CALIPSO satellite. The values in this field are identical to the values in the Lidar_Data_Altitudes SDS and are retained in V5.00 for backward compatibility with existing software.

Met_Data_Altitudes

Altitudes (above mean sea level) at which the 33 element profiles of ancillary meteorological data are reported. The values in this field are identical to the values in the Met Data Altitudes SDS and are retained in V5.00 for backward compatibility with existing software.

Rayleigh Extinction_Cross-section_532

This field reports the 532 nm Rayleigh extinction cross-section (5.167e-31 m^2) used to construct model molecular attenuated backscatter profiles from the MERRA-2 temperature and pressure data.

Rayleigh_Extinction_Cross-section_1064

This field reports the 1064 nm Rayleigh extinction cross-section (3.127e-32 m^2) used to construct model molecular attenuated backscatter profiles from the MERRA-2 temperature and pressure data.

Rayleigh_Backscatter_Cross-section_532

This field reports the 1064 nm Rayleigh backscatter cross-section (5.930e-32 $m^2 \cdot sr^{-1}$) used to construct model molecular attenuated backscatter profiles from the MERRA-2 temperature and pressure data.

Rayleigh_Backscatter_Cross-section_1064

This field reports the 1064 nm Rayleigh backscatter cross-section (3.592e-33 $m^2 \cdot sr^{-1}$) used to construct model molecular attenuated backscatter profiles from the MERRA-2 temperature and pressure data.

Ozone_Absorption_Cross-section_532

This field reports the 532 nm ozone absorption cross-section (2.728461e-25 m^2) used to construct model molecular attenuated backscatter profiles from the MERRA-2 temperature and pressure data.

Ozone_Absorption_Cross-section_1064

This field reports the 1064 nm ozone absorption cross-section that would be used to construct model molecular attenuated backscatter profiles from the MERRA-2 temperature and pressure data. Because ozone attenuation is negligible at 1064 nm, ozone two-way transmittances are not used when creating the 1064 nm molecular model profiles, so the cross-section value is set to 0.00 m^2.

ScatteringRatioIn532NightCalibrationRegion

Assumed scattering ratio in the 532 nm nighttime calibration region. The value is 1.01. See Kar et al., 2018 for details.

ScatteringRatioIn532NightCalibrationRegionUncertainty

Assumed scattering ratio uncertainty in the 532 nm nighttime calibration region. The value is 0.01. See Kar et al., 2018 for details.

MolecularModelUncertainty

The relative uncertainty assumed in the molecular model used for 532 and 1064 nm calibration, derived from estimates of the uncertainties in the MERRA-2 temperature profiles (e.g., as in Campbell et al., 2015). This value is fixed throughout the mission at 0.015.

CirrusBackscatterColorRatio

Cirrus cloud color ratio assumed by the 1064 nm calibration algorithm. The metadata incorrectly reports this value as 1.00, whereas the correct value is 1.01. See Vaughan et al., 2010 for details.

CirrusBackscatterColorRatioUncertainty

Cirrus cloud single sample color ratio uncertainty assumed by the 1064 nm calibration algorithm. The value is 0.25. See Vaughan et al., 2010 for details.

AutocorrelationCoefficientFile

This 160-byte character field reports the name of the auto-correlation coefficient file used in production.

Data Release Information

At the conclusion of the mission, the CALIPSO project had released five major versions of the lidar level 1 data products, as well as several minor version updates. Table 10 lists all major and minor releases.

Table 10: Release date, version number, date range, and production strategy for all CALIOP level 1 data products

Lidar Level 1: Half orbits (Night and Day)			
Release Date	**Version**	**Data Date Range**	**Production Strategy**
October 2025	5.00	June 13, 2006 to June 30, 2023	Standard
June 2023	4.51	June 13, 2006 to June 30, 2023	Standard
October 2020	4.21	July 01, 2020 to January 19, 2022	Standard
October 2018	4.20	June 13, 2006 to June 20, 2020	Standard
November 2016*	4.10	June 13, 2006 to September 30, 2020	Standard

Lidar Level 1: Half orbits (Night and Day)			
Release Date	**Version**	**Data Date Range**	**Production Strategy**
October 2020*	3.41	October 1, 2020 to June 30, 2023	Validated Stage 1
December 2016	3.40	December 1, 2016 to September 31, 2020	Validated Stage 1
April 2013	3.30	March 1, 2013 to November 30, 2016	Validated Stage 1
December 2011	3.02	November 1, 2011 to February 28, 2013	Validated Stage 1
May 2010	3.01	June 13, 2006 to October 31, 2011	Validated Stage 1
October 2008	2.02	September 14, 2008 to October 29, 2009	Provisional
January 2008	2.01	June 13, 2006 to September 13, 2008	Provisional
December 2006	1.10	June 13, 2006 to November 11, 2007	Provisional / Beta

* to allow timely production of browse images, V3.41 and V4.10 standard data products were distributed concurrently from 1 October 2020 through the end of the mission

Data Quality Information

Data Quality Statement for the Version 5.00 Lidar Level 1B Product

Lidar Calibration Coefficients

The procedures used for the radiometric calibration of the 532 nm and 1064 nm channels in the version 5.00 (V5.0) release of the CALIOP level 1b profile product are identical to those used in the previous release (version 4.51). So too are all procedures used to calibrate the polarization gain ratio (PGR). The one change that will yield small differences in the radiometric calibration coefficients is a modification to the energy normalization scheme applied in the level 1 processing. The V5.0 data averaging engine now correctly identifies and compensates for intermittent occurrences of low energy laser pulses. For an arbitrarily selected month when the laser was healthy (March 2010; 680, 293, 770 samples) all PGRs were exactly identical in the V4.51 and V5.00. For the radiometric calibration coefficients, 86.7% of the 532 nm values were exactly identical in the two data sets, as were 85.5% of the 1064 nm values. Maximum differences are on the order of ±0.06%. On the other hand, for an arbitrarily selected month when the laser was malfunctioning (September 2022; 673, 687, 755 samples), the PGRs are once again identical but there are more pronounced (albeit still mostly small) differences in the calibration coefficients. Descriptive statistics of the quotient of the V5.0 values divided by the V4.51 values are shown the Table 11.

Table 11: Descriptive statistics of the ratios of the V5.0 and V4.51 calibration coefficients (V5.0 divided by V4.51) for two arbitrarily chosen months. The sample count for March 2010, when the CALIPSO laser was behaving nominally, is 680, 293, 770. For September 2022, when the laser was emitting relatively high rates of low energy pulses, the sample count is 673, 687, 755. While there are some large outliers in the September 2022 data, 98.4% of all V5.0 calibration coefficients remain within ±2% of their V4.51 values.

	March 2010			September 2022		
	C_{532}	C_{1064}	PGR	C_{532}	C_{1064}	PGR
Min	0.9995	0.9995	1.0000	0.9396	0.9400	1.0000
Max	1.0006	1.0006	1.0000	1.0844	1.0847	1.0000
Median	1.0000	1.0000	1.0000	1.0028	1.0029	1.0000
MAD	0.0000	0.0000	0.0000	0.0034	0.0035	0.0000
Mean	1.0000	1.0000	1.0000	1.0032	1.0033	1.0000
St. Dev.	0.0000	0.0000	0.0000	0.0055	0.0055	0.0000

Lidar Reflectance Retrievals

The calibration coefficients used to retrieve reflectances from CALIOP's RMS baseline measurements are changed significantly in V5.0. CALIOP V5.0 reflectances are calibrated relative to exactly collocated CALIPSO wide field-of-view camera (WFC) reflectances for measurements acquired above deep convective ice clouds. While CALIOP and the WFC operate at a different wavelengths (532 nm and 645 nm, respectively), reflectances from dense ice clouds are known to be spectrally independent at these wavelengths (e.g., Doelling et al., 2013). The calibration equation relating CALIOP RMS baseline measurements to WFC reflectances is

$$K = \frac{\rho_{WFC}\, S_0 \cos(\theta)\, D}{\pi\left(RMS_{\parallel}^2 + Q \times RMS_{\perp}^2\right)}$$

with notation as described in Table 12.

Table 12: Interpretation of the notation used in the CALIOP reflectance calibration equation.

variable	Description
ρ_{WFC}	Bi-directional reflectance measured by CALIPSO's wide field-of-view camera
RMS_x	Root mean square of the CALIOP backscatter signals in the 65–80 km baseline region for the 532 nm parallel (x = ∥) and perpendicular (x = ⊥) channels. Since molecular and particulate scattering at these altitudes is essentially zero, the RMS baseline values provide a measure of the background signal levels in each channel. Their sum is directly related to the total upwelling radiance.
Q	Gain normalization factor that equalizes the gains between the two polarization channels in the lidar. $$Q = \left(\frac{G_{\parallel}}{G_{\perp} \times PGR}\right)^2$$ where G_x represents the amplifier gains in the parallel and perpendicular channels and PGR is the polarization gain ratio.
S_0	Extra-terrestrial solar irradiance over the lidar bandpass. In all previous data releases, S_0 was fixed at 2027.04 W m^{-2} µm^{-2}. For the CALIOP V5.0 release, S_0 is set to a constant value of 1920 W m^{-2} µm^{-2}, consistent with the results given in Figure 4 of Gueymard, 2018.
θ	Solar zenith angle
D	Earth-sun distance

Figure 5 uses daytime data acquired during all of March 2010 to illustrate the changes made by adopting this new calibration strategy.

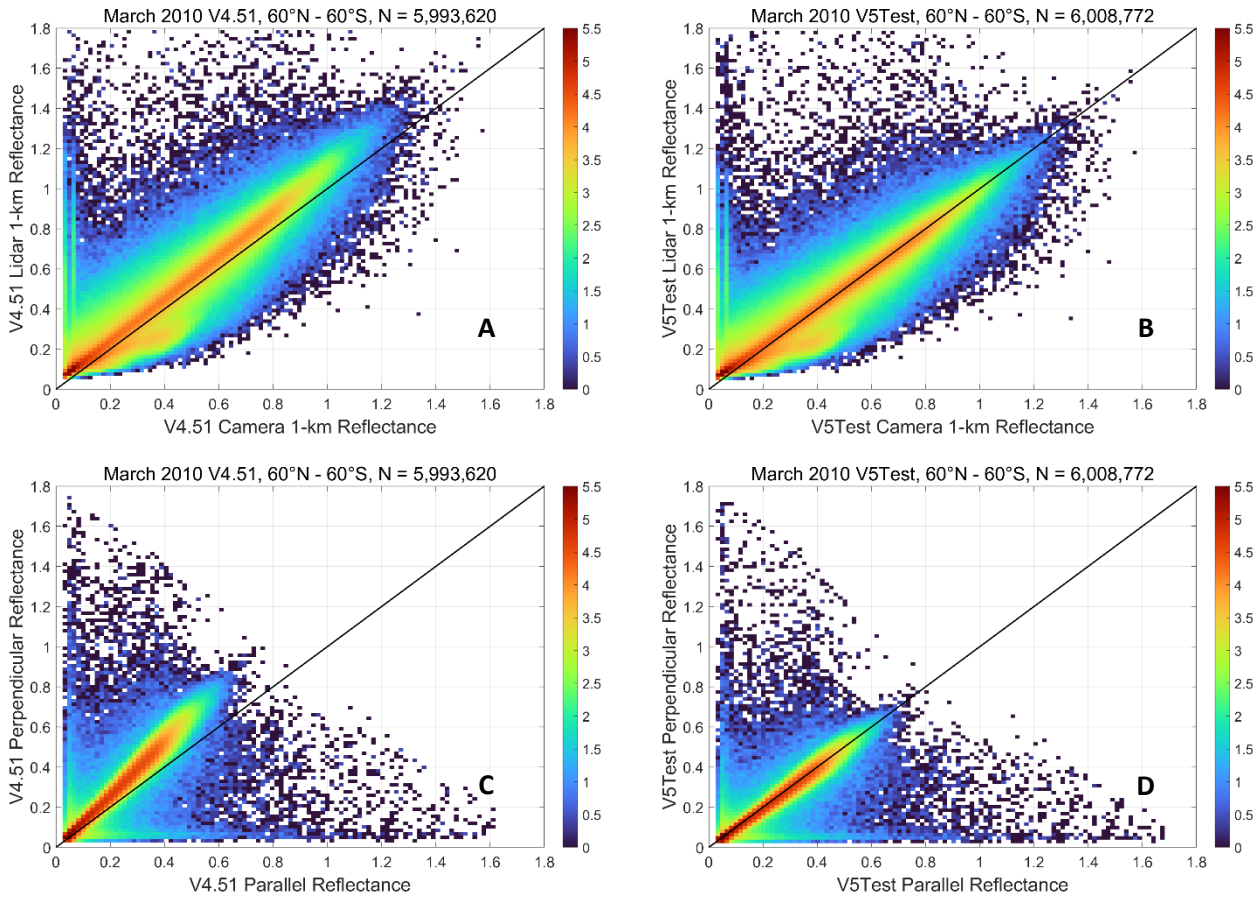

Figure 5. Panel A shows the V4.51 distribution of lidar-retrieved reflectances versus the reflectances measured by the WFC for March 2010. As the reflectances increase in magnitude, lidar values are seen to increasingly overestimate the WFC measurements. This increase is counter to physical expectations, which dictate that as the reflectances grow larger and almost wholly dominated by measurements of opaque ice clouds, the reflectances should become spectrally independent and hence converge to equal values for both sensors. This expectation is realized in Panel B, which shows the V5.0 distribution of lidar-retrieved reflectances versus the reflectances measured by the WFC for March 2010. Panels C and D compare the magnitudes of the parallel (x-axis) and perpendicular (y-axis) components of the lidar-derived reflectances for, respectively, V4.51 and V5.0. Because the background measurements acquired above opaque ice clouds are almost entirely depolarized, the reflectances measured in the parallel and perpendicular channels should be essentially identical. While this is clearly not the case in panel C, panel D shows that this expectation is fully satisfied for the V5.0 reflectances.

Figure 6 compares the V5.0 lidar-derived reflectances to collocated reflectances measured in MODIS band 4 (545–565 nm).

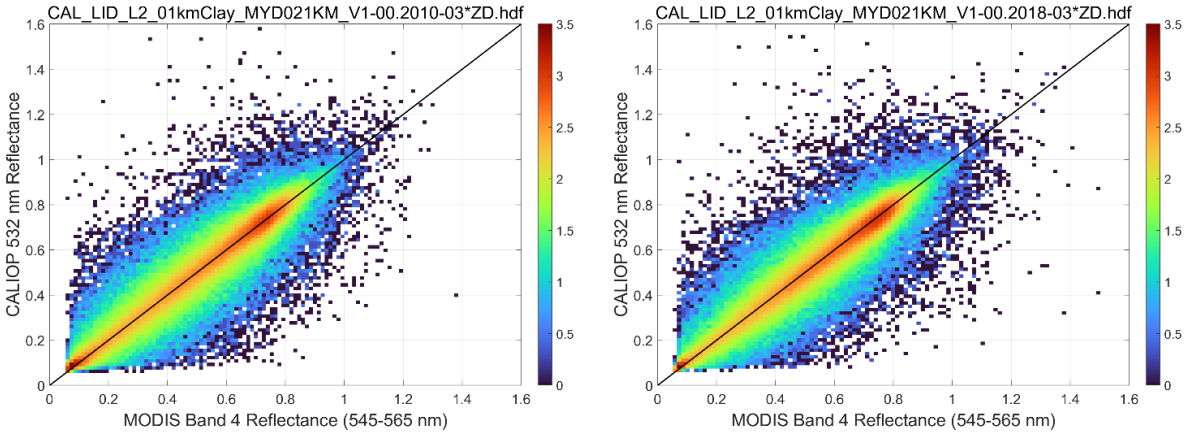

Figure 6. The left panel compares CALIOP 532 nm reflectances to MODIS band 4 reflectances for all collocated pixels observed during March 2010. Similarly, the right panel compares CALIOP reflectances to MODIS band 4 reflectances for all collocated pixels observed during March 2018. Although noisy, the one-to-one correspondence between the two sets of measurements is quite clear. The left panel data can be compared directly to the results shown in all panels of Figure 5.

Lidar Reflectance Uncertainties

Lidar reflectance calibration coefficients are calculated for all daytime observations using CALIOP and WFC data for which the solar zenith angle was less than 70°. Both lidar and camera data are averaged to a 1 km along track resolution. Calculations are restricted to profiles containing high confidence (80 ≤ CAD score ≤ 100) ice clouds that are opaque at single shot resolution. These data selection requirements delivered 6626 ± 2997 calibration opportunities per calendar day. Because daily aggregates typically contain several large outliers, the reflectance calibration coefficient assigned for each calendar day is the daily median of all samples acquired. Similarly, the estimated uncertainties are the daily median absolute distances (MADs). To reduce the random noise in the calibration coefficients and associated uncertainties, the calibration time series is smoothed using a 31-day running median. To avoid underestimating the calibration uncertainties, the magnitudes of the 31-day smoothed MADs were further increased by a factor of 1.2. A time series of the calibration coefficients used to derive the V5.0 reflectances is shown in Figure 7.

The CALIPSO WFC suffered a terminal malfunction in March 2021. After that date, reflectance calibration coefficients and their uncertainties are extrapolated from the available estimates using polynomial approximations.

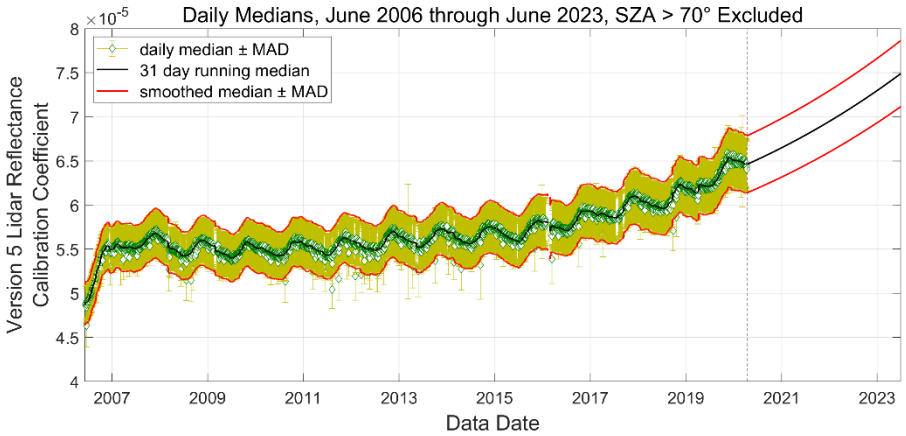

Figure 7. Full mission timeline showing daily medians ± MADs (pale green diamonds with tan error bars) of the lidar reflectance calibration coefficients. The 31-day running median of the daily medians is shown as a dark green line. Red lines show the 31-day running median ± 1.20 times the 31-day running MAD.

The equations for deriving the reflectances in the parallel and perpendicular channels can be written as

$$\rho_{\parallel} = W \times RMS_{\parallel}^2$$

$$\rho_{\perp} = W \times Q \times RMS_{\perp}^2$$

so that the total column reflectance is $\rho = \rho_{\parallel} + \rho_{\perp} = W\,(RMS_{\parallel}^2 + Q \times RMS_{\perp}^2)$, with Q as define above and

$$W = \frac{\pi\, K}{S_0\, \cos(\theta)\, D}$$

Reflectance uncertainties are estimated using standard propagation of errors techniques; i.e.

$$\left(\frac{\partial \rho_{\parallel}}{\rho_{\parallel}}\right)^2 = \left(\frac{\partial W}{W}\right)^2 + \left(\frac{\partial RMS_{\parallel}^2}{RMS_{\parallel}^2}\right)^2$$

and

$$\left(\frac{\partial \rho_{\perp}}{\rho_{\perp}}\right)^2 = \left(\frac{\partial W}{W}\right)^2 + \left(\frac{\partial Q}{Q}\right)^2 + \left(\frac{\partial RMS_{\perp}^2}{RMS_{\perp}^2}\right)^2$$

These values are reported in, respectively, the Parallel_Column_Reflectance_Uncertainty_532 SDS and the Perpendicular_Column_Reflectance_Uncertainty_532 SDS. Reflectance uncertainties were not calculated in previous data releases, and thus these SDSs were uniformly populated with fill values.

Lidar Browse Images

Beginning September 15, 2022, with granule ID 2022-09-15T08-37-02, the final portions of the nighttime browse images for earlier version included regions of missing data at the end of each orbit. This error, now corrected in V5.0, occurred due to a misconfiguration of the browse image plotting code that failed to account for CALIPSO's drifting orbit in the C-Train. This change only affects the browse images created and distributed by the CALIPSO project and has no impact at all on any of the CALIPSO data products.

Newly Added Scientific Data Sets (SDSs)

The V5.0 lidar level 1b data product introduces the following new SDSs:

a. Lidar Data Altitudes – in previous versions of the CALIPSO data products, the fixed altitude array that identified the heights above mean sea level for the range bins in the profile SDSs was located in the file metadata. In the V5.0 files, a second copy of the altitude array is included as an SDS (Lidar_Data_Altitudes).

b. Met Data Altitudes – as with the lidar data altitudes, the fixed altitude array that identified the heights above mean sea level for the ancillary meteorological data was previously located only in the file metadata. In the V5.0 files, a second copy is also included as an SDS (Met_Data_Altitudes).

c. Reflectance Calibration Coefficient @ 532 nm – for the first time, the V5.0 lidar level 1b profile products include an SDS (Reflectance_Calibration_Coefficient_532) that reports the calibration coefficients used to derive the 532 nm reflectance estimates.

d. Reflectance Calibration Coefficient Uncertainty @ 532 nm – also for the first time, reflectance calibration coefficient uncertainties are reported in an SDS (Reflectance_Calibration_Coefficient_Uncertainty_532) now included in the V5.0 data release.

Update Format of CALIPSO HDF Files

The V5.0 CALIPSO data products are distributed as Hierarchical Data Format Version 4 (HDF4) files, consistent with the EOS requirement in effect when CALIPSO launched in 2006. Since launch, there have been substantial technological advances in data discoverability and access resources. To make CALIPSO data more readily accessible

to the scientific community beyond the life of the mission and take advantage of newer data access capabilities, several modifications were made to the format and content of the CALIOP HDF files. These include:

- Updating all units to conform to NetCDF Climate and Forecast (CF) metadata conventions.
- Ensuring that all dimensions are named, to allow HDF to netCDF conversions using commercial off the shelf (COTS) tools that currently exist.
- Creating/expanding SDS attributes and comments to make the data products more self-documenting.

Updated Colormaps for the CALIOP Browse Images

A revised set of CALIOP browse images is released in V5.0 with colormaps that improve readability for individuals with color vision deficiencies (CVD) for key CALIOP observables (Vaillant de Guélis et al., 2025). This includes new browse images for volume depolarization ratio and all three attenuated backscatters, building upon the CVD-friendly color ratio browse imagery introduced in V4.5.

Legacy colormaps used for volume depolarization ratio and color ratio in previous data releases could at times inhibit the ability to accurately interpret changes in magnitude, making quantitative analysis challenging. This was especially true for individuals with CVD where several colors in the legacy colormaps are difficult to distinguish from one another. To improve the readability of CALIOP imagery for these observables, new colormaps are introduced in V5.0 that are perceptually sequential to better represent changes in magnitude and use colors that are separable for individuals with CVD. The new depolarization ratio colormap replaces the legacy colormap in V5.0 browse images.

The new colormap for attenuated backscatter builds upon the strengths of the legacy colormap. It retains three backscattering regimes to resolve detail within the range of magnitudes required for scientific interpretation. Similar colors are used, but green is eliminated to avoid red-green ambiguities for individuals with CVD. Transitions between the three regimes are softened to reduce the appearance of false boundaries in the atmosphere that were prevalent in the legacy colormap. Lastly, the lower backscatter limit is reduced by an order of magnitude, allowing weakly backscattering particulate features to be resolved from the molecular background, particularly in the 532 nm perpendicular channel browse images. Due to the widespread use of the legacy attenuated backscatter colormap by the scientific community, the V5.0 data release will continue to include attenuated backscatter browse images using this colormap. Browse images using the new colormap will also be released in V5.0 as a CVD-friendly alternative.

Data Quality Statement for the Version 4.51 Lidar Level 1B Product

Data Version: **4.51**
Data Release Date: **June 1, 2023**
Data Date Range: **June 13, 2006 to June 30, 2023**

Version 4.51 lidar level 1B (L1B) data product continues to rely on the 532 nm and 1064 nm radiometric calibration techniques used previously in the version 4.0 (released March 2014) and version 4.1 (released November 2016) L1B data. The derivation of the polarization gain ratio (PGR) has been updated to repair a coding error that introduced an elevated bias in the nighttime PGR calibration and to address observed PGR differences between daytime and nighttime. These PGR revisions are the most pervasive changes in the V4.51 L1B release. Based on analyses of on-orbit extended background measurements, the 1064 nm baseline shape correction was revised to characterize the phase of very low-level signal oscillations more accurately. Finally, data handling modifications made in the V4.51 L1B release now enable the calibration algorithms to recognize and accommodate the slow degradation of instrument performance observed over the course of the 16-plus year mission. Thus, the 532 nm daytime and 1064 nm calibration approaches were updated to minimize the impact of low energy laser pulses.

These changes to the V4.51 lidar level 1B products are described in more detail below:

Polarization Gain Ratio Corrections

The PGR is an estimated relative gain between the parallel and perpendicular 532 nm detectors and is needed to derive the 532 nm total attenuated backscatter (β′) and volume depolarization ratio (δ_v) (Powell et al., 2009). This can be seen in equations 1 and 2, expressed as a function of altitude (z), calibration coefficient (C), and uncalibrated, range-corrected, gain and energy normalized backscatter measurements (X(z)) acquired in the 532 nm parallel (‖) and perpendicular (⊥) channels.

$$\beta'(z) = \beta'_{\parallel}(z) + \beta'_{\perp}(z) = \frac{1}{C}\left(X_{\parallel}(z) + \frac{X_{\perp}(z)}{PGR}\right) \quad (1)$$

$$\delta_v(z) = \frac{X_{\perp}}{PGR \cdot X_{\parallel}(z)} \quad (2)$$

In earlier versions, the PGR was treated as a diurnally invariant system parameter that was assumed to change slowly as a function of mission elapsed time. PGR values are updated every 6 to 8 weeks by placing CALIOP in a special PGR calibration configuration for the duration of a single nighttime orbit segment.

The V4.51 PGR calculations incorporate two changes relative to previous versions. First, differences had previously been noted in the PGR calibrations derived from the science data (X-Band) used in V4.1 data production when compared against estimates computed from the near-real-time engineering data (S-Band), with X-Band values underestimating the S-Band values by 4% - 6%. This bias was eliminated by correcting an error in the X-Band code that mistakenly used only positive parallel and perpendicular signals. Additionally, a new filtering routine now eliminates contributions to the averaged signals arising from low energy laser pulses (see section 3 below). The reduction of this bias can be seen in Figure 1, in which the new V4.51 PGR estimates (in red) are considerably lower than the V4.1 value (in blue) and now more closely match the independent estimates derived from the S-Band data (in yellow).

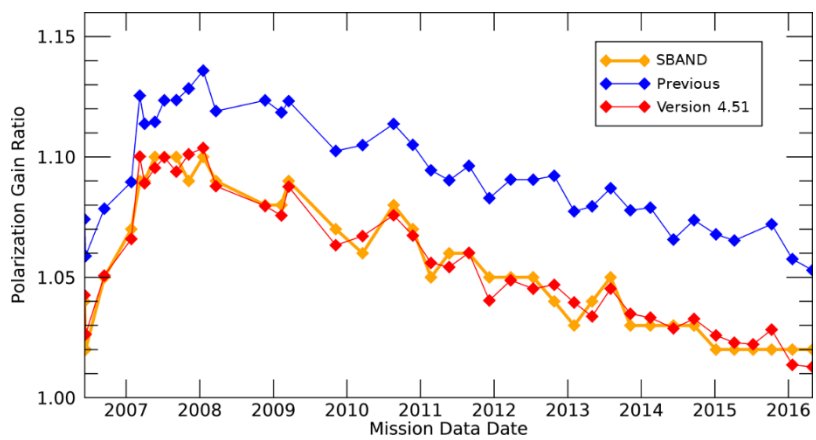

Figure 1: Polarization gain ratio (PGR) estimated from the pre-V4.5 X-Band (blue) used to generate previous versions of the CALIOP level 1 and level 2 data products. PGR estimates built from the S-Band (yellow). Revised X-Band PGR (red) used to generate the new V4.51 level 1 night-side data product.

In 2016, spurred by user feedback that noted unexpected differences between nighttime and daytime depolarization ratios seen in the lidar level 2 (L2) data (Sassen et al., 2012), CALIOP began conducting occasional extended PGR calibration operations. For these extended ops, CALIOP remains in its PGR calibration configuration for multiple days, and hence acquires PGR calibration data during both the nighttime and daytime portions of each orbit. Contrary to prelaunch expectations, but consistent with user reports, the PGR estimates obtained during these procedures showed very clear day-night differences, with progressive transition from night-to-day values at the terminators. Reproducing these diurnal calibration differences led to the second major change in the V4.51 PGR estimates. While the nighttime PGR calibration technique remains the same as in earlier data releases, during daytime CALIOP now implements the approach of Liu et al., 2004, who pioneered the use of solar background measurements above optically thick, strongly scattering cirrus clouds to estimate the relative gains of the parallel

and perpendicular measurement channels. To minimize the effects of outliers and intermittent data outages, daily mean daytime PGRs are smoothed using a 21-day running mean prior to use in the L1B and L2 data analyses. The differences between the daytime and nighttime PGRs used in CALIOP's V4.51 data release is illustrated in Figure 2. Additional details on the V4.51 daytime PGR calibration technique are given in Vaughan et al., 2023.

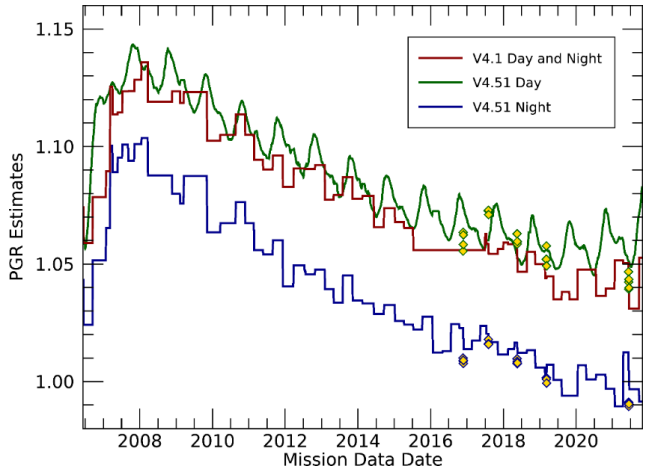

Figure 2: Polarization gain ratios (PGR) over the CALIPSO mission used in V4.1 and earlier (red), in V4.51 day (green), and in V4.51 night (blue). The estimated day and night PGRs during extended polarization calibration operations are shown as filled diamonds.

1064 nm Baseline Shape Correction

Baseline shapes are the profiles measured when CALIOP is in full data acquisition mode but without the laser firing; i.e., they represent the state of the system when no laser backscatter is present. After launch of CALIPSO, the baseline shapes characterized using laboratory measurements for 532 nm and 1064 nm channels were compared with on-orbit background measurements. This comparison showed that while the lab-derived 532 nm baseline shape accurately represented the on-orbit behavior, derived, the 1064 nm shape was slightly out of phase. Figure 3 shows how the pre-launch baseline (green) deviates in phase when compared baseline shape measurements acquired in 2014, 2015, and 2016. To alleviate this issue, new 1064 nm baseline shapes were constructed based on on-orbit measurements for both the primary and secondary lasers. The results of these efforts also shown in Figure 3 confirm that the changes to the 1064 nm baseline shape now accurately map to the onboard digitizer counts.

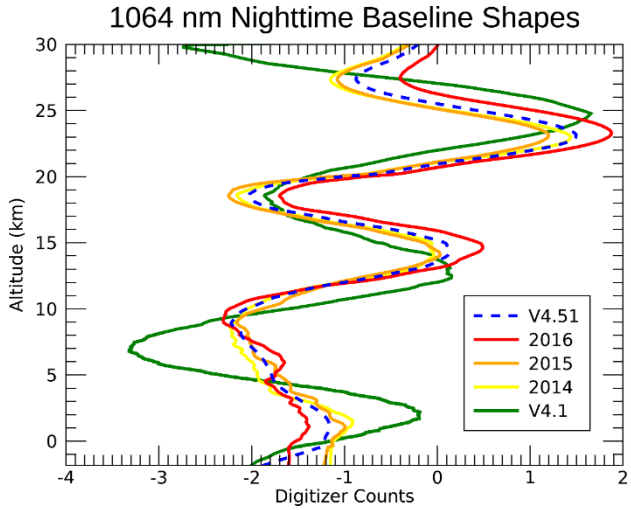

Figure 3: The 1064 nm night-time baseline shapes for pre-launch (green) and post-launch derived from extended background measurements in 2014 (yellow), 2015 (orange), and 2016 (red). Pre-launch baseline shapes were applied to V4.1 data and earlier. The new baseline shape (dashed blue) was derived from the extended background

measurements and is applied the backup laser (March 12, 2009, to current). A different baseline shape was built for measurements made in 2006 by the primary laser (June 13, 3006 to February 19, 2009).

532nm (daytime) and 1064nm Calibration Mitigation for Low Laser Energies

Data having unusually low laser pulse energies, particularly those observed within the SAA, have been effectively filtered out as part of the multi-orbital averaging scheme used by both the 532 nm daytime and the 1064 nm calibration techniques. For the first 10 years of the mission (2006-2016) this approach worked well, as the calibration and calibration uncertainties tracked expected estimates derived during algorithm development. Starting in late 2016 it was observed and publicly reported that there were noticeable increases in the frequency and global distribution of these low energy shots. Further, this increase in low energy shots began to negatively impact the quality of the L2 data. To address this problem, the V4.2 L2 product was released in October 2018, with additional science data set (SDS) records included that allowed users to exclude affected L2 data.

Initially, the L1B 532 nm daytime and 1064 nm calibration coefficients were not affected by this deterioration in laser energies. Over time, however, measurable changes in the variability of the calibration coefficients and a substantial increase in the calibration coefficient uncertainties were observed at latitudes corresponding to the SAA. Due to CALIOP's multi-orbit calibration averaging schemes (Kar et al., 2018; Getzewich et al., 2018; Vaughan et al., 2019), these calibration perturbations extend to longitudes well outside the SAA. These phenomena are not seen in the 532 nm nighttime calibration, which includes a strict SNR filter that effectively eliminates contamination by low energy laser pulses.

The impact to 532 nm daytime calibration was corrected by employing a newly developed low energy mitigation (LEM) algorithm (Tackett et al., 2025). The LEM algorithm detects and removes low energy laser pulses while accounting for differing on-board averaging regimes (Hunt et al., 2009). This is crucial to accurately account for signals that are averaged differently as a function of altitude, rather than just filtering on a per-profile basis. Application of this LEM filtering technique decreases the variability of the daytime calibration coefficients and magnitudes of the uncertainties, particularly within the latitudes directly impacted by the SAA. This reduction is demonstrated in Figures 4 and 5 for data acquired during November 2020. Figures 4(A) and 4(B) show curtains of calibration coefficients expressed as a function of granule elapsed time (y axis) and data day (x axis). Comparing these two images illustrates the dramatic reduction in calibration variability achieved within the SAA in V4.5. The change in relative calibration uncertainty in Figure 4(C) also captures this reduction. Although there is still some uncertainty in V4.5, due primarily to the reduction in sampling incurred by low energy filtering, it is demonstrably much less than in V4.1. Figures 5(D) and 5(F) also show the reduction in variability of the daytime calibration coefficients at SAA latitudes, with a measured zonal increase of 2% peaking along the SAA latitude band. Just as importantly, Figures 5(A), 5(B), and 5(C) confirm that, as expected, there is no change in the 532 nm nighttime calibration between V4.1 and V4.51.

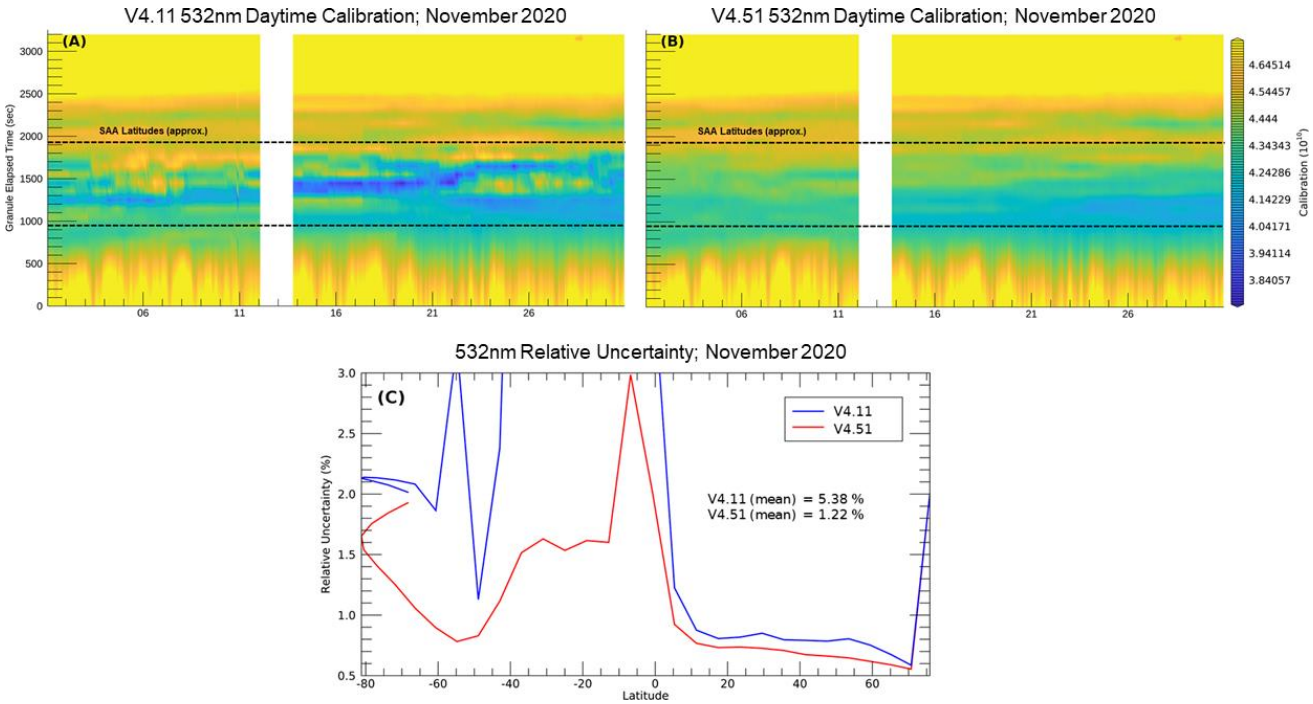

Figure 4: November 2020 Lidar Level 1 532nm daytime calibration coefficient and calibration relative uncertainty for V4.11 (A, C blue) and V4.51 (B, C red). The calibration coefficients (A, B) are shown as a function of granule elapsed time (y-axis) and day of the month (x-axis). The gap in data between November 12-13, 2020, was due to the payload being commanded to SAFE mode, during which no data was collected.

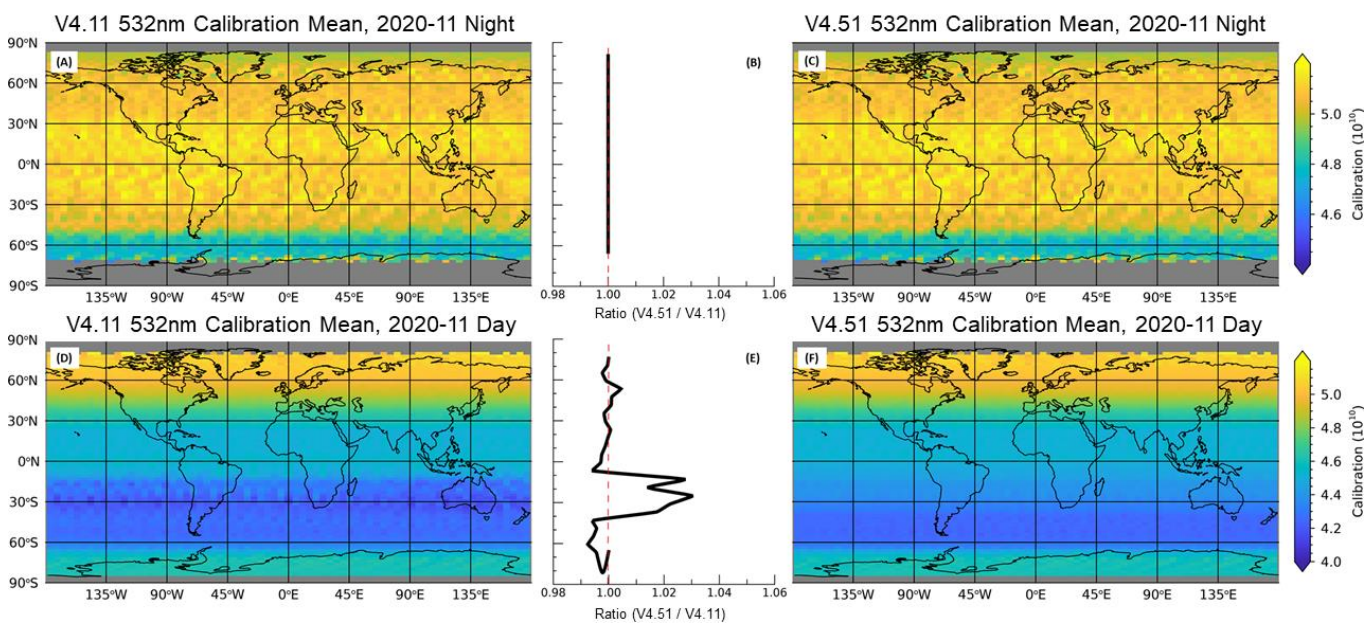

Figure 5: November 2020 Lidar Level 1 532nm night (A-C) and day (D-F) calibration between V4.11 and V4.51. Zonal ratios between V4.51 and V4.11 are also seen for night (B) and day (E).

The new daytime calibration distributions now fall within the expected bounds developed by the CALIOP science impact testing (SIT) team. These bounds are one part of a collection of quality assurance metrics first established during initial V4 development and now used to continuously monitor the quality of the CALIOP calibration coefficients prior to data release. The revised calibrations and uncertainties are now commensurate with the calibration coefficients and associated uncertainties that were recorded prior to the increased frequency of low

laser energy shots since 2016. The LEM algorithm will be adapted to correct the L2 data products for low energy shots in a future data release, after the V4.51.

Unlike the 532 nm daytime calibration technique, which relies on high-altitude backscatter normalization in clear air regions, the 1064 nm calibration technique uses backscatter measured in cirrus clouds. The 1064 nm calibration algorithm identifies appropriate cirrus clouds based on a set of selection criteria computed using data averaged over 15 laser pulses (Vaughan et al., 2019). Because low laser energies can markedly degrade the accuracy of this cirrus identification scheme, the V4.51 algorithm now specifically rejects all candidate targets for which the laser energy of any of the 15 pulses averaged fails to exceed 0.01 joules. Improvements to the daytime 1064 nm calibration coefficient uncertainties are also expected given the changes to the daytime 532 nm calibration coefficient uncertainties previously noted. The results of these efforts, in combination with the changes also attributable to the PGR and 532nm daytime calibration updates previously noted, are seen in Figure 6. Figure 6 (A-C) shows a general reduction in the 1064 nm night-time calibration coefficients from V4.1 to V4.51, which is attributable to the decrease in the night-time PGR. Conversely the concentrated increase at the SAA latitude band, beyond the influence of the PGR, is due to the discarding of low energy shots. Figure 6 (D-F) shows a zonal increase of 1064 nm daytime calibration from V4.1 to V4.51 of ~1% due to changes to the daytime PGR, with a progressive transition to night-time values near the terminators. The exception to this is at the SAA latitudes, where the 1064nm daytime calibration coefficients are increased by 5%, which is attributable to the combined effects of the changes to the PGR (~1%), the changes to the 532nm daytime calibration coefficients (~3 %) and low energy shot mitigation changes (~1 %).

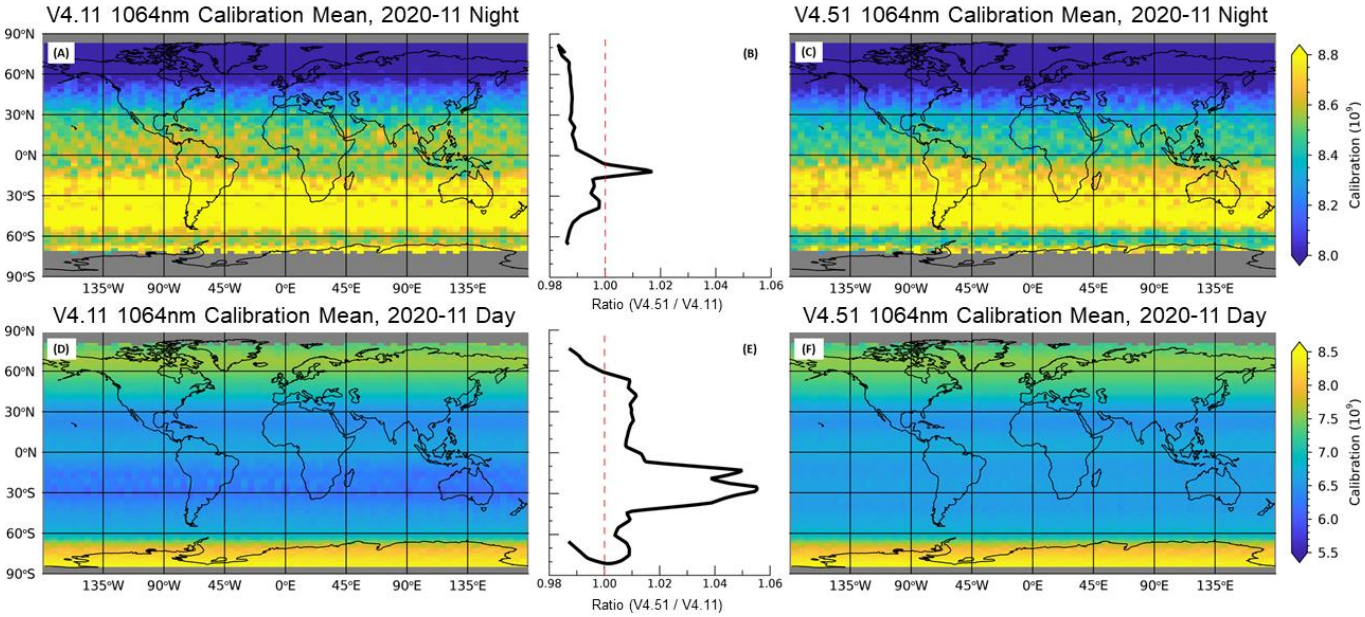

Figure 6: November 2020 Lidar Level 1 1064nm night (A-C) and day (D-F) calibration between V4.11 and V4.51. Zonal ratios between V4.51 and V4.11 are also seen for night (B) and day (E).

Data Quality Statement for the Version 4.11 Lidar Level 1B Product

Version 4.11 reflects a change in the data products due to a required upgrade to the operating system on the CALIPSO production cluster. All algorithms were re-compiled to process in this new environment with no change to the underlying science algorithms or inputs.

Data Quality Statement for the Version 4.10 Lidar Level 1B Product

Version 4.10 (V4.10) lidar level 1B data products are produced using the same greatly improved calibration algorithms that were first incorporated in the version 4.00 (V4.00) release in March 2014 (see below). The improvements in V4.10 release are in the ancillary data used for surface detection and calibration. The GTOPO30

Digital Elevation Model (DEM) used in V4.00 has been replaced by a substantially more accurate DEM developed by the CloudSat project. The Global Modeling and Assimilation Office (GMAO) Forward Processing for Instrument Team (FP-IT) meteorological forecast product has been replaced with the higher quality Modern Era Retrospective-Analysis for Research (MERRA-2) reanalysis product.

These changes to the V4.10 lidar level 1B products are described in more detail below:

Updated Digital Elevation Map (DEM)

Surface elevation has been referenced to the GTOPO30 DEM since beginning of the CALIPSO mission. Many inaccuracies with surface elevation have been identified, especially over Greenland and Antarctica and in remote mountainous areas. To address these differences, and to complement improvements to the surface detection techniques in the new level 2 products, GTOPO30 has been replaced with a new DEM developed by the CloudSat team. Use of the CloudSat DEM will also allow both missions to have a common surface reference. Pre-release analysis has shown a marked improvement in CALIPSO level 2 surface detection accuracy as a result of using the new DEM.

Inclusion of MERRA-2 Data

Increased accuracy and reliability of CALIOP calibration is achieved by replacing the Global Modeling and Assimilation Office (GMAO) Forward Processing for Instrument Teams (FP-IT) global meteorological product with the Modern Era Retrospective-Analysis for Research (MERRA-2) product. MERRA-2 assimilates temperature measurements from the Microwave Limb Sensor (MLS) on Aura, whereas the FP-IT distribution does not. The corrections provided by the MLS assimilation yield improved calibration coefficients, particularly in the polar regions. Analysis between current GMAO and MERRA-2 showed very little difference in ozone number densities, but measurable differences in molecular densities. The differences in molecular densities have been observed not to exceed 5%, but are focused particularly in high southern latitudes, and reflect changes in the temperatures reported in MERRA-2 relative to FPIT.

Data Quality Statement for the Version 4.00 Lidar Level 1B Product

Version 4.00 reflect substantial changes in the data product to include:

532 nm Nighttime Calibration

Significant changes were made in the CALIOP 532 nm nighttime calibration algorithm used in version 4.00. In the previous versions, this calibration was carried out by molecular normalization in the altitude range of 30-34 km, assuming the near absence of aerosols at these altitudes (Powell et al., 2009). However, it has now been demonstrated that the aerosol loading in this region is larger than pre-launch expectations, particularly in the tropics (Vernier et al., 2009). Because the version 3 calibration made no allowance for these aerosols, biases (i.e., overestimates) were introduced into the calibration coefficients for the 532 nm nighttime data and these biases subsequently propagated into the 532 nm daytime and 1064 nm day and nighttime data. In version 4, the molecular normalization is applied at 36-39 km, which is near the upper limit of the CALIOP measurements. Independent data from SAGE II and GOMOS indicate this region is almost entirely free of particulates. To counter the loss of signal-to-noise ratio incurred by moving to the higher calibration altitude, the version 4 calibration algorithm now averages data over multiple nighttime granules (i.e., orbit segments). The relative uncertainties of the calibration coefficients are on the order of 1-2% overall, with the highest values occurring over the South Atlantic Anomaly and the polar regions. Owing to a coding error discovered in the version 3 calibration software, the 532 nm nighttime calibration uncertainties reported in the version 3 data products underestimated the actual uncertainties by a factor of ~3. This bug has been eliminated in the version 4 software.

The revised calibration approach produces a decrease of the zonal mean calibration coefficients by ~3% overall as compared to the version 3.x values. This in turn leads to an increase in the total attenuated backscatter coefficients by the same amount. The attenuated scattering ratios (ASR) in the 30-34 km region are now increased by up to 5%

over previous versions, indicating seasonal variations which are consistent with the predictions of Vernier et al., 2009. Stratospheric aerosol loading at these altitudes is now clearly captured by CALIOP measurements, showing up as spatial structures which are consistent with stratospheric dynamics. Similarly, the clear-air scattering ratios at 8-12 km which showed an anomalous dip (ASR < 1) in the tropics in the version 3.x data products now no longer do so. Version 3 showed extended areas in the polar regions with ASR < 1. Improved data filtering strategies in the version 4 calibration region have now largely removed these anomalies found in the previous versions.

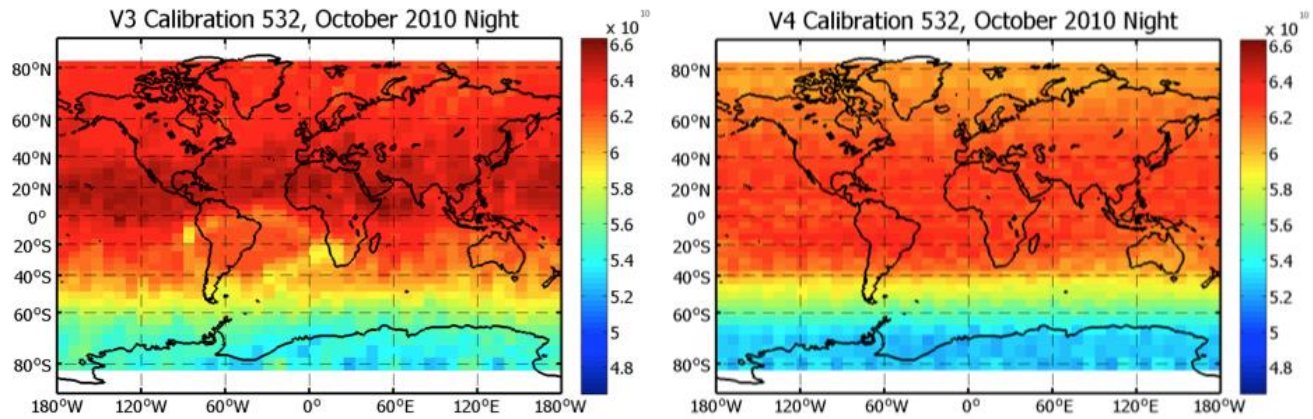

Figure 1: monthly mean 532 nm calibration coefficients for October 2010 nighttime measurements. Calibration coefficients computed for the version 3.01 data release are shown at left. Calibration coefficients computed in pre-release testing of the version 4.0 algorithm are shown at right.

Figure 1 shows nighttime monthly mean 532 nm calibration coefficients for October 2010 computed for version 3.01 (left) and for a pre-release test of the version 4.00 algorithm (right). In the version 3.01 data, the presence of the stratospheric aerosol layer in the tropics is clearly visible as a region of high calibration coefficients located between the equator and 20° N. The South Atlantic Anomaly (SAA) is also visible as an oval of reduced calibration coefficients centered at ~20° S and ~40° W. By contrast, neither of these geophysical features appears in the version 4.00 data. In both images, the diminution of the calibration coefficients in the southern hemisphere, as the satellite approaches the night-to-day terminator, is indicative of changes in the on-board thermal environment that perturb the alignment between the laser transmitter and receiver. The median reduction in the calibration coefficients from version 3.01 to version 4.00 is ~3%.

532 nm Daytime Calibration

The 532 nm daytime calibration is obtained by referencing the uncalibrated daytime signal to the calibrated nighttime signal in spatially matched regions where the diurnal variability in the background aerosol loading is assumed to be non-existent (Powell et al., 2010). This night-to-day calibration transfer region has been raised to a higher altitude in version 4 to avoid clouds and increase the number of samples used in calculating daytime calibration coefficients. With version 4 the transfer region is still 4 km deep, as with previous versions, but it now follows on top of the 400 K isentropic surface which is always above the tropopause and above the meteorologically active part of the atmosphere (Hoskins 1991), thus better satisfying the assumption that there is no diurnal variability in the transfer region. Version 4 daytime 532 nm calibration coefficients in the troposphere are ~5% smaller compared to those in version 3 due to a commensurate reduction in nighttime calibration coefficients. Subsequently, attenuated scattering ratios (or equivalently attenuated backscatter coefficients) are now higher in the troposphere by a few percent with largest increases of ~5% near the poles (Figure 2c).

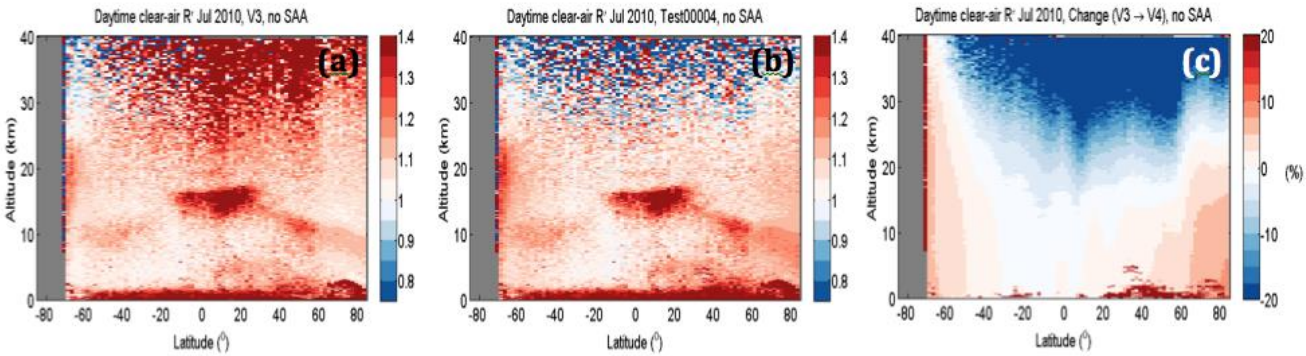

Figure 2: Daytime clear-air attenuated scattering ratios for July 2010 in (a) version 3 and (b) version 4. Panel (c) shows the percent change in daytime clear-air attenuated scattering ratios from version 3 to version 4 (red indicates an increase). The South Atlantic Anomaly has been excluded.

A new correction has also been added to the level 1 processing of the two 532 nm channels in the daytime to increase the accuracy of measurements at high altitudes where signal levels are low. While the correction is small, its relative effect is significant at high altitudes where the backscatter signal is also small. Consequently, the correction has reduced the overestimate of scattering ratios at high altitudes in version 3 (Figure 2a), making the average attenuated scattering ratio in this region equal unity in version 4 as expected (Figure 2b).

In the version 3 release, the agreement between day and night clear-air attenuated scattering ratios at high altitudes was poor and varied with latitude, possibly due to diurnal variability in aerosol loading and clouds reducing the potential number of clear-air samples in the 8-12 km version 3 calibration transfer region (Figure 3a). Version 4 shows a marked improvement in the agreement between day and night clear-air attenuated scattering ratios above the version 4 calibration transfer region (to within 1 ± 3%), demonstrating (1) the validity of assuming that there is no diurnal variability in stratospheric aerosol loading at these altitudes, (2) that the day/night agreement of clear-air attenuated scattering ratios holds even above the night-to-day calibration transfer region where they are forced to agree, and (3) the version 4 calibration procedure adjusts for differences in day and night instrument behavior.

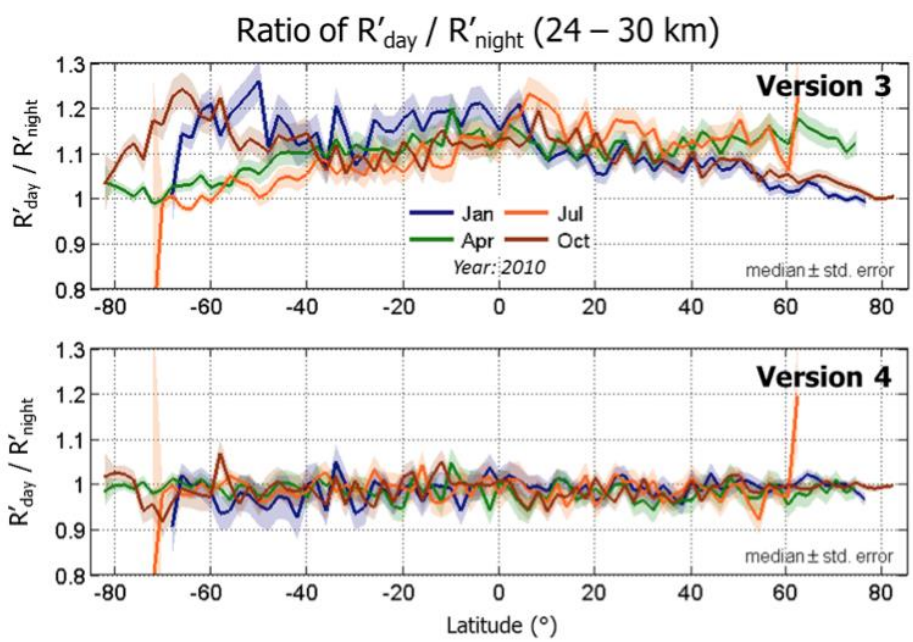

Figure 3: Ratio of day to night clear-air attenuated scattering ratios R' at 24 - 30 km in (a) version 3 and (b) version 4 for January, April, July, and October 2010. The South Atlantic Anomaly has been excluded.

The coarse estimates of daytime calibration uncertainties provided in version 3 have been replaced in version 4 with improved estimates derived using rigorous error propagation. Random uncertainties in the daytime calibration coefficients are less than 1% at all latitudes except near the poles and are typically smaller than the corresponding nighttime calibration uncertainties because many more samples are averaged for the daytime calibrations. The version 4 calibration uncertainty estimates are continuous across the day-night terminators, and the daytime calibration uncertainties increase near the poles in version 4 to merge smoothly with their nighttime counterparts.

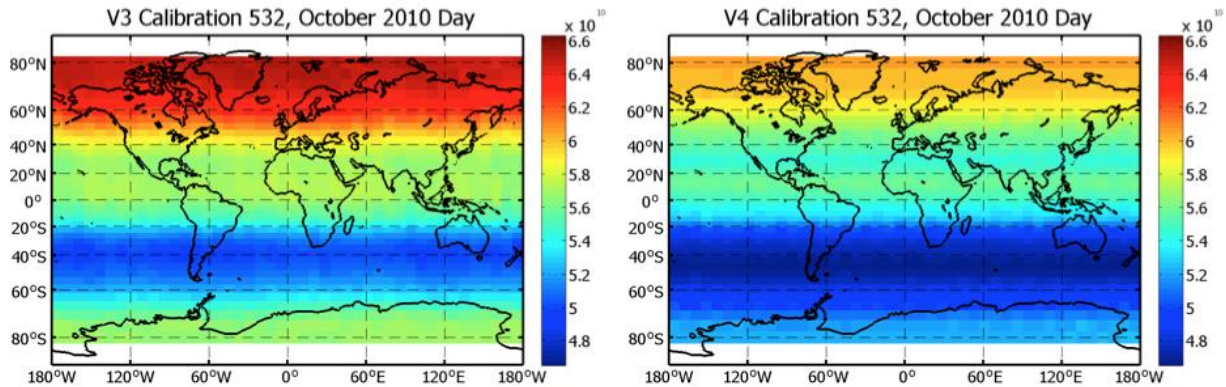

Figure 4: monthly mean 532 nm calibration coefficients for October 2010 daytime measurements. Calibration coefficients computed for the version 3.01 data release are shown at left. Calibration coefficients computed in pre-release testing of the version 4.0 algorithm are shown at right.

Figure 4 shows daytime monthly mean 532 nm calibration coefficients for October 2010 computed for version 3.01 (left) and for a pre-release test of the version 4.00 algorithm (right). The median reduction in the calibration coefficients from version 3.01 to version 4.00 is ~6%.

1064 nm Daytime and Nighttime Calibration

Version 4 includes substantially redesigned algorithms for the 1064 nm daytime and nighttime calibrations (Vaughan et al., 2019). The CALIOP 1064 channel does not have sufficient molecular backscatter to allow referencing to clear air at high altitudes, so instead a scale factor is computed to match the 1064 nm signals from cirrus clouds to the corresponding 532 nm signals, with the assumption that the 1064/532 backscatter ratio from cirrus should be close to 1. The 1064 nm calibration coefficient is then the product of this 1064 nm scale factor and the 532 nm calibration coefficient. In Version 4, these 1064 nm scale factors are calculated and applied as a function of the granule elapsed time, to better represent the relative variations of the 532 and 1064 signals along orbit segments. The criteria for selecting the cirrus clouds that are used in the scale factor calculation have also been changed significantly in Version 4 (Vaughan et al., 2019). The new criteria provide a larger number of cloud samples in the southern latitudes, and remove water clouds, many polar stratospheric clouds and very thin cirrus from the reference ensemble. Accuracy of the 1064 nm calibrated attenuated backscatter is thus much improved over CALIOP Version 3 by minimizing latitudinal variation caused by measurement artifacts, and by selecting reference targets that can more reasonably be expected to have a 1064/532 signal ratio that is close to unity.

Figure 5 illustrates the changes in the 1064 nm scale factor between version 3 (left) and version 4 (right) for both nighttime data (top row) and daytime data (bottom row) for the month of October 2010. The version 3 scale factors show a large discontinuity between the very high nighttime values and the very low daytime values, along with abrupt changes in value between adjacent orbit segments. The version 4 scale factors, on the other hand, vary smoothly as a function of orbit elapsed time, with continuous values at both terminators. The magnitudes of the changes from V3 to V4 in the nighttime mean scale factors range between 20% lower (northern hemisphere) to 7% higher (southern hemisphere), with the median nighttime difference being 6% lower. The daytime mean scale

factors range between 14% lower (northern hemisphere) to 19% higher (southern hemisphere), with the median daytime difference being 3% lower.

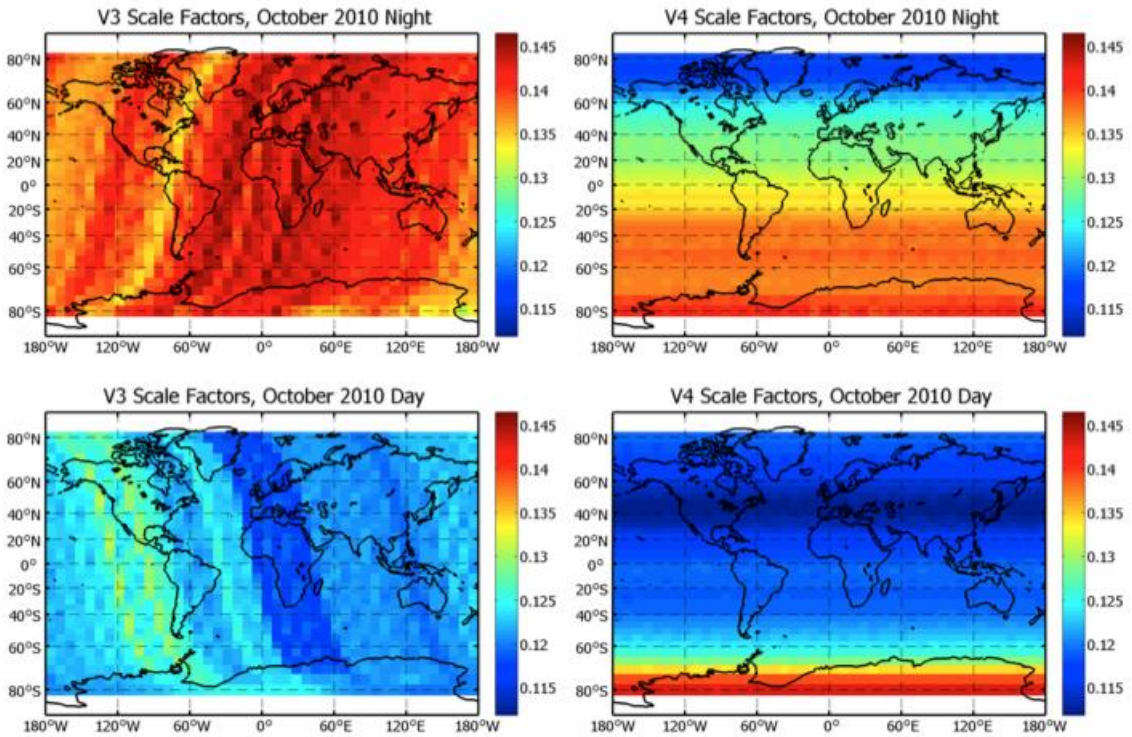

Figure 5: monthly mean 1064 nm calibration scale factors for October 2010. Version 3 scale factors are shown on the left; version 4 scale factors are shown on the right. The upper panels show nighttime data and the lower panels show daytime data.

Figure 6 illustrates the changes in the 1064 nm calibration coefficients between version 3 (left) and version 4 (right) for both nighttime data (top row) and daytime data (bottom row) for the month of October 2010. The data in the top row of Figure 6 represents the 532 nm nighttime calibration coefficients shown in Figure 1 multiplied by the nighttime 1064 nm calibration scale factors shown in the top row of Figure 5. Similarly, the data in the bottom row of Figure 6 represents the 532 nm daytime calibration coefficients shown in Figure 4 multiplied by the daytime 1064 nm calibration scale factors shown in the bottom row of Figure 5. The version 3 1064 nm calibration coefficients exhibit spatial artifacts and irregularities that arise from both the version 3 532 nm calibration coefficients and from the version 3 1064 nm scale factors. In contrast to the version 3 data, the version 4 1064 nm calibration coefficients produced by the new calibration and scale factor algorithms are seen to vary smoothly both latitudinally and longitudinally. The magnitudes of the changes from V3 to V4 in the nighttime mean 1064 nm calibration coefficients range between 22% lower (northern hemisphere) to 8% higher (southern hemisphere), with the median nighttime difference being 8% lower. The daytime mean 1064 nm calibration coefficients range between 20% lower (northern hemisphere) to 10% higher (southern hemisphere), with the median daytime difference again being 8% lower.

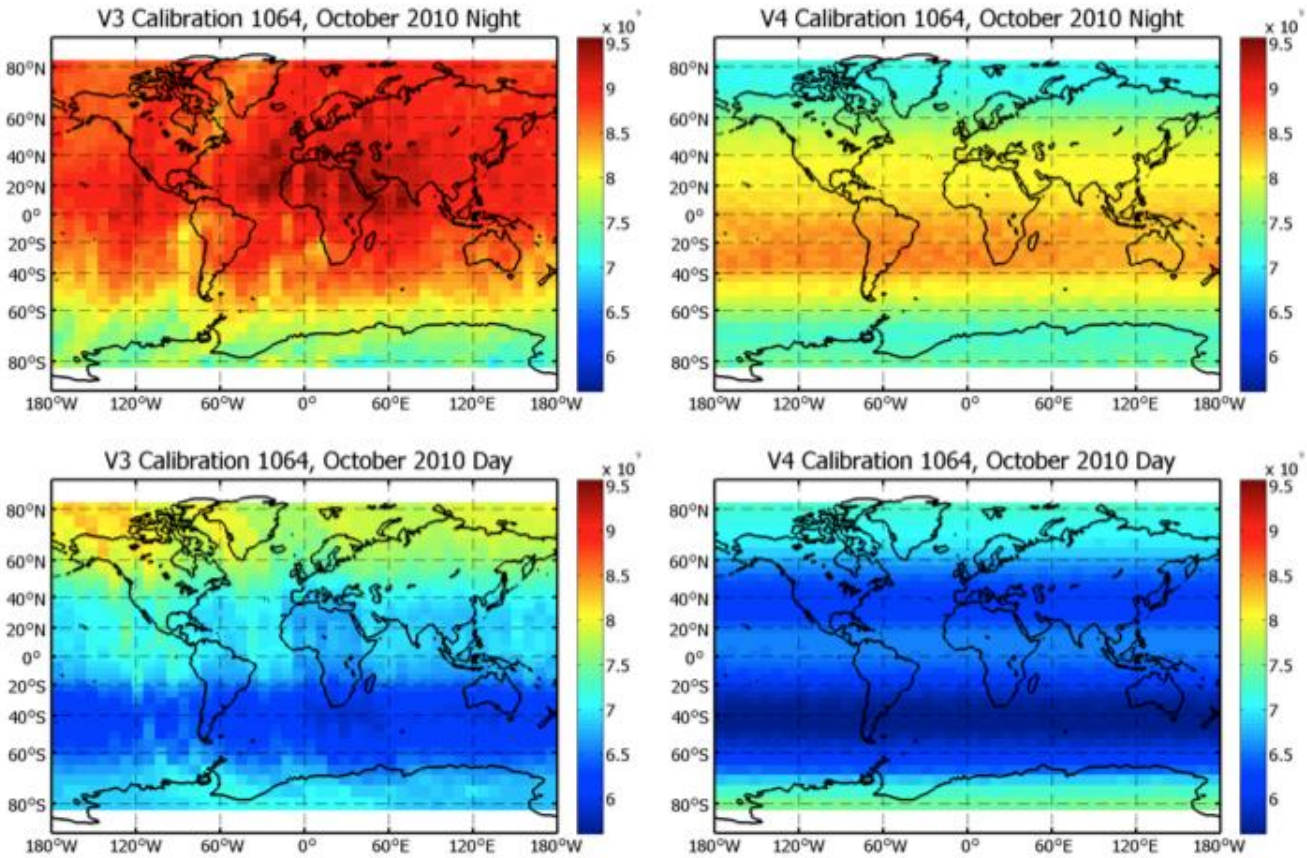

Figure 6: monthly mean 1064 nm calibration coefficients for October 2010. The 1064 nm calibration coefficients are the product of the 532 nm calibration coefficients and the 1064 nm scale factors. Version 3 calibration coefficients are shown on the left; version 4 calibration coefficients are shown on the right. The upper panels show nighttime data, and the lower panels show daytime data.

<u>QC Flag 2</u>

The rules for setting the bits in QC Flag_2 have been revised to provide more accurate indications of bad data. As of version 4.00,

- a value of 0 in any bit indicates good data.
- a value of 1 in bits 11-16 always indicates bad data.
- for all other bits, a value of 1 indicates data values outside the normally expected range, which may or may not indicate bad data.
    - Occasional randomly occurring values of 1 are generally due radiation-induced noise spikes, and do not indicate bad data. These will be most frequent when passing through the South Atlantic Anomaly.
    - Except as noted below, a value of 1 that persists for several minutes is probably an indication of bad data and should be investigated before using the data.
    - A value of 1 in bits 20-22 may indicate the presence of Polar Stratospheric Clouds. These occur only in the polar winter and may persist for more than 10 minutes. They do not indicate bad data.

New Surface Parameters

Nine new parameters describing the properties of the surface return were added to the version 4 lidar level 1B data product:

- Surface_Saturation_Flag_532Par
- Surface_Saturation_Index_532Par
- Negative_Signal_Anomaly_Index_532Par
- Surface_Saturation_Flag_532Perp
- Surface_Saturation_Index_532Perp
- Negative_Signal_Anomaly_Index_532Perp
- Surface_Saturation_Flag_1064
- Surface_Saturation_Index_1064

Surface_Saturation_Flag_xxxx:

The version 4 level 1 analysis includes a new algorithm to estimate the likelihood that the signal return from the planetary surface is saturated. This information is reported separately for each of the three measurement channels using an 8-bit integer whose value indicates the likelihood that the surface backscatter signal is saturated.

Surface_Saturation_Index_xxxx:

This SDS is a 16-bit integer used to identify the altitude array index of the maximum signal value for cases where Surface_Saturation_Flag_xxxx is either Possibly_Saturated or Certainly_Saturated. For cases where the Surface_Saturation_Flag_xxxx is Not_Saturated, the Surface_Saturation_Index_xxxx is set to -1. Otherwise, values will lie in the range between 277 (at ~8.2 km) and 577 (at -0.5 km).

Level 1B data users who use the surface signal to derive optical depths are advised that the values recorded in the lidar level 1B attenuated backscatter data may substantially under-represent the true signal values whenever the Surface_Saturation_Flag_xxxx is either Possibly_Saturated or Certainly_Saturated.

Negative_Signal_Anomaly_Index_xxxx:

A phenomenon, dubbed a “negative signal anomaly”, occurs when the level 1B attenuated backscatter becomes anomalously negative at the onset of an abrupt, strongly scattering target such as the planetary surface or a dense cloud. This effect can occur in any of the three lidar channels and is present in all versions of the CALIOP level 1B product. At this time only one range bin is believed to be affected in profiles containing the anomaly. Additional documentation is provided in the CALIPSO Data User’s Guide. The cause of the negative signal anomaly is currently under investigation by the CALIPSO team. Occurrences of this phenomenon are reported using a 16-bit integer in the Negative_Signal_Anomaly_Index_xxxx SDS. For those profiles where the negative surface anomaly is not present, the Negative_Signal_Anomaly_Index_xxxx is set to -1. Otherwise, values will lie in the range between 277 (at ~8.2 km) and 577 (at -0.5 km).

Level 1B data users are advised to exclude from their analyses attenuated backscatter in range bins identified by the Negative Signal Anomaly Index. Users of the 532 nm total attenuated backscatter data should consider the Negative Signal Anomaly Index for both parallel and perpendicular channels.

Data Quality Statement for the Version 3.41 Lidar Level 1B Product

Version 3.41 reflects a change in the data products due to a required upgrade to the operating system on the CALIPSO production cluster. All algorithms were re-compiled to process in this new environment with no change to the underlying science algorithms or inputs.

Data Quality Statement for the Version 3.40 Lidar Level 1B Product

Version 3.40 data products reflect a transition of the Global Modeling and Assimilation Office (GMAO) Forward Processing – Instrument Teams (FP-IT) meteorological data version from 5.9.1 to 5.12.4.

Data Quality Statement for the Version 3.30 Lidar Level 1B Product

Version 3.30 data products incorporate updated Global Modeling and Assimilation Office (GMAO) Forward Processing – Instrument Teams (FP-IT) meteorological data, and the enhanced Air Force Weather Authority (AFWA) Snow and Ice Data Set as ancillary inputs to the production of these data sets, beginning with data date March 1, 2013.

Impacts on CALIOP data products caused by the transition to GEOS-5 FP-IT are predicted to be minimal, based on a comparison of CALIOP Version 3.02 against CALIOP Version 3.30.

Level 1B nighttime calibration: GEOS-5 molecular number densities in the CALIOP nighttime calibration region increased by roughly 0.6% on average which caused the nighttime calibration coefficients to decrease on average by -0.6%. Since attenuated backscatter is inversely proportional to the calibration coefficient, nighttime attenuated backscatter will increase by 0.6% on average.

Level 1B daytime calibration: GEOS-5 molecular number densities in the CALIOP daytime calibration region increased by 0.1% near the equator and increased by up to 0.4 - 0.7% near the poles which caused daytime calibration coefficients to decrease by <-0.2% near the equator and decrease by roughly -0.8% near the poles. Daytime attenuated backscatters will thereby increase by these same magnitudes.

Data Quality Statement for the Version 3.02 Lidar Level 1B Product

Version 3.02 represents a transition of the Lidar, IIR, and WFC processing and browse code to a new cluster computing system. No algorithm changes were introduced, and very minor changes were observed between V 3.01 and V 3.02 as a result of the compiler and computer architecture differences.

Data Quality Statement for the Version 3.01 Lidar Level 1B Product

Version 3.01 includes corrections to the 532 nm and 1064 nm extinction, backscatter, and ozone cross-sections that were applied in the release of Lidar Level 1B Version 3.00. The data were reprocessed using the corrected values and are being released as Version 3.01.

The following six parameters were added in the file metadata:

- Rayleigh Extinction Cross-section 532
- Rayleigh Extinction Cross-section 1064
- Rayleigh Backscatter Cross-section 532
- Rayleigh Backscatter Cross-section 1064
- Ozone Absorption Cross-section 532
- Ozone Absorption Cross-section 1064

Data Quality Statement for the Version 3.00 Lidar Level 1B Product

Version 3.00 includes algorithm improvements, modifications to existing data parameters, and new data parameters. The maturity level of Version 3.00 Lidar Level 1B data product is assigned Validated Stage 1. In this stage, all obvious errors have been identified and corrected, and intercomparisons of attenuated backscatter products have been performed at selected locations and times.

Algorithm improvements were implemented for:

- 532-nm daytime calibration : A revised 532-nm daytime calibration algorithm produces improved corrections to the thermally induced drift in signal level that occurs over the course of the daytime orbit segment. In

Version 3.00, the empirically determined correction factors are applied using a 34-point linear approximation as compared to the 5-point linear approximation implemented in Versions 2.01 and 2.02. This allows for better characterization of the small-scale changes in signal level that take place over the daytime orbit segment. Comparisons of nighttime and newly calibrated daytime clear air attenuated scattering ratios over 8-12 km in altitude were made for multiple seasons of LOM 2 (first laser) operation and for the first three months of LOM 1 (backup laser) operation. In all cases the agreement between night and day was within 5% for the entire orbit segment.

- laser energy calculations and signal normalization by laser energy : Two updates to the 532-nm and 1064-nm laser energy calculation algorithm were implemented in Version 3.00 in order to reduce errors in both calibration and the processing of signal profiles for low energy laser shots. The first update uses new laser energy conversion coefficients to improve the accuracy of the laser energy calculation. In the second update, the signal normalization by laser energy is changed to normalize by averaging region instead of by shot. That is, for each averaging region, normalize all averaged shots by the corresponding average energy for that region. Data are averaged on-board over 15, 5, 3, or 1 shot(s) before downlink, with the amount of averaging depending upon the altitude. Application of the new normalization scheme improves the signal normalization for frames with low energy laser shots and has little effect on frames with nominal laser energies.
- interpolation of GMAO gridded data products to the CALIPSO orbit tracks : Corrections were made to the code used to interpolate the GMAO gridded data products to the CALIPSO orbit tracks. In Versions 2.01 and 2.02, two bracketing GMAO files were used to derive meteorological parameters. In some cases, the CALIPSO measurement times fell outside of the bracketing file times causing parameters to be extrapolated. In Version 3.00, this problem was rectified by selecting three GMAO files for each orbit track segment. This assures the orbit track times are completely contained within the GMAO data file times.

The modified parameters are:

- Met_Data_Altitudes : The altitudes reported in the parameter Met_Data_Altitudes was modified so they are now coincident with an altitude reported in the Lidar_Data_Altitudes array.
- QC_Flag and QC_Flag_2 : The quality flags QC_Flag and QC_Flag_2 was updated to identify the profiles that were normalized using low energy.

New data parameters describe the orbit and path number and are included in the file metadata. The following six parameters were added:

- Orbit_Number_at_Granule_Start
- Orbit_Number_at_Granule_End
- Orbit_Number_Change_Time
- Path_Number_at_Granule_Start
- Path_Number_at_Granule_End
- Path_Number_Change_Time

Data Quality Statement for the Version 2.02 Lidar Level 1B Product

Version 2.02 of the CALIOP Level 1 data products is a maintenance release that implements the following changes. Corrections were made to the code used to interpolate the GMAO gridded data products to the CALIPSO orbit tracks. As a result, the magnitudes of the molecular and ozone number densities used in the Level 1 calibration algorithms can be different from the values used in the version 2.01 processing by as much as ±0.5%. The exact magnitude of the changes encountered will vary according to latitude, longitude, altitude, and season. A small (~0.8%) error was corrected in the calculation of the Cabannes backscattering cross-sections used to derive the molecular scattering models used for the Level 1 532 nm parallel channel calibration algorithm. Combined, these

two changes yield 532 nm calibration constants that are larger, on average, by ∼1%, with a corresponding decrease in the magnitudes of the 532 nm attenuated backscatter coefficients. Similar effects occur in the 1064 nm data. Implementing these changes increases the agreement between collocated measurements of "clear air" acquired by CALIPSO and NASA's high spectral resolution lidar (HRSL) by ∼1%.

Data Quality Statement for the Version 2.01 Lidar Level 1B Product

Version 2.01 includes revised algorithms for the 532 nm daytime calibration and the 1064 nm daytime and nighttime calibration. The 532 nm daytime calibration coefficients are now scaled relative to systematic variations in the measured backscatter signal that occur over the course of the daytime orbit segments. The Version 2.01 532 nm daytime calibration corrections produce significant improvements to the overall quality of both the Lidar Level 1 and 2 daytime data products, particularly in the northern hemisphere where the Level 1 data contain significant daytime calibration biases. It is recommended to use the Version 2.01 for all analyses of the 532 nm daytime data. The Version 2.01 1064 nm calibration coefficients also vary as a function of orbit elapsed time, in the same manner and for the same reasons as the 532 nm calibration constants. In all previous versions, a single value for the 1064 nm calibration coefficient was computed and applied for each daytime and nighttime orbit granule. The revised calibration procedures produce substantial improvements in the quality of the 1064 nm measurements. These changes are most noticeable in the daytime granules. Use of the Version 2.01 data products is recommended for all analyses that rely on the 1064 nm measurements.

Data Quality Statement for the Version 1.22 Lidar Level 1B Product

Beginning with Version 1.22, the lidar altitude array is calculated as a function of the spacecraft off-nadir angle. The off-nadir parameter used during processing is determined by the tilt of the CALIPSO lidar relative to nadir and is limited to 0.3 degrees or 3.0 degrees. In Versions prior to 1.22, the off-nadir parameter was set to a constant 0.3 degrees. The lidar altitude array is stored in the HDF metadata field named "Lidar Data Altitude". Since the beginning of operations in June 2006, CALIPSO has been operating with the lidar pointed at 0.3 degrees off-nadir (along track in the forward direction) with the exception of November 7-17, 2006 and August 21 to September 7, 2007. During these periods, CALIPSO operated with the lidar pointed at 3.0 degrees off nadir. Beginning November 28, 2007, the off-nadir angle will be permanently changed to 3.0 degrees. When comparing data acquired at 3.0 degrees and 0.3 degrees, the altitude difference between two adjacent samples is relatively insignificant, but when summed over the entire backscatter region, the difference is significant. The total span at 3.0 degrees is 57 meters less than it is at 0.3 degrees. It is therefore important to retrieve the altitude array stored within the HDF metadata field in order to maintain the correct altitude registration between data acquired at different off-nadir angles. The method used to register the 532 nm and 1064 nm backscatter coefficients to the lidar altitude array is changed beginning with Version 1.22. In previous versions, altitude registration was performed by interpolating the lidar profile data to the lidar altitude array. Beginning with Version 1.22, the lidar altitude registration is performed without interpolation. For all versions, the altitudes corresponding to all backscatter samples are re-computed during level 1 processing, making use of postprocessed ephemeris data and measured attitude data. Using the recomputed altitudes, the backscatter data are then re-mapped to the original fixed altitude array. In versions 1.0 through 1.21, the attenuated backscatter value that is placed in a given altitude bin is a linear combination of the two attenuated backscatter values whose recomputed altitudes are on either side of that bin's altitude. In versions 1.22 and forward, the interpolation has been eliminated and the attenuated backscatter value of the lowest altitude sample is reassigned to the altitude bin most closely matching its recomputed altitude value. The remaining attenuated backscatter coefficients are then assigned sequentially to the fixed altitude array bins from that bin upward. This approach has the virtue of leaving the highest resolution attenuated backscatter values unmodified. The final step averages the lidar profiles stored at the fixed 30-meter resolution altitude to the downlink resolution. Two surface parameters are added in Version 1.22. The parameter named Surface_Altitude_Shift contains the altitude difference between the profile specific 30-meter altitude array and the fixed 30-meter altitude array at the array element that includes mean sea level. The units are in kilometers and the values may be positive or negative. The difference is calculated as: Surface_Altitude_Shift = altitude (profile specific 30-meter mean sea level bin) - altitude (fixed 30-meter mean sea level bin). The parameter named Number_Bins_Shift contains the number of 30-meter bins the profile specific 30-meter array elements are shifted to match the lowest altitude bin of the fixed 30-

meter altitude array. The profile specific array elements may be shifted up or down. Four column reflectance parameters are added in Version 1.22. The parameters named Parallel_Column_Reflectance_532 and Perpendicular_Column_Reflectance_532 contain the 532 nm parallel and perpendicular bi-directional column reflectance values derived from the lidar background measurements, respectively. The parameters named Parallel_Column_Reflectance_Uncertainty_532 and Perpendicular_Column_Reflectance_Uncertainty_532 are the 532 nm parallel and perpendicular column reflectance uncertainties, respectively.

Data Quality Statement for the Version 1.20 Lidar Level 1B Product

The Global Modeling and Assimilation Office (GMAO) next generation global atmospheric model, Goddard Earth Observing System Model, Version 5 (GEOS-5), was implemented within the CALIPSO Data Processing System on March 1, 2007. The CALIOP Level 1B data products obtained from the GEOS-5 assimilation model include Molecular Number Density, Ozone Number Density, Temperature, and Pressure. The four GMAO-5 meteorological parameters are used to compute the CALIOP Level 1B data for the 532 nm and 1064 nm calibration constants and their associated uncertainties. The CALIOP Level 1B calibration constant data products are named Calibration Constant 532 and Calibration Constant 1064. The CALIOP Level 1B calibration constant data product uncertainties are named Calibration Constant Uncertainty 532 and Calibration Constant Uncertainty 1064. The CALIOP Level 1B 532 nm total and perpendicular and 1064 nm attenuated backscatter profiles are derived from the calibrated (divided by calibration constant), range-corrected, laser energy normalized, baseline subtracted lidar return signal. Thus, the following CALIOP Level 1B data products are also affected by the GEOS-5 transition: Total Attenuated Backscatter 532, Perpendicular Attenuated Backscatter 532, and Attenuated Backscatter 1064. Version 1.20 is a provisional data release. A preliminary comparison of the CALIOP Level 1B calibration constants and uncertainties computed using GEOS-4 and 5 was performed and revealed small differences. Uncertainties and possible biases will be documented when the data are validated. The CALIOP Level 1B data products prior to March 1, 2007 (June 5, 2006, to February 28, 2007) were processed using GEOS-4. These data will be reprocessed using GEOS-5 and are planned to be released in the Fall of 2007.

Data Quality Statement for the Version 1.11 Lidar Level 1B Product

A software fix was applied to the Lidar Level 1B Profile code to correct a memory allocation error that caused jobs to terminate prematurely. The science algorithm and code did not change. Because this version update has no impact on the data products being generated, the Data Quality Statement for Version 1.11 is the same as for Version 1.10, Initial Release.

Data Quality Statement for the Version 1.10 Lidar Level 1B Product

Geolocation and altitude registration have been checked and appear to have uncertainties of less than the sampling resolution (333 m for geolocation and 30 m for altitude). Random uncertainties due to noise in the 532-nm parallel channel calibration, 1064-nm channel calibration and polarization gain ratio (PGR) determination have been assessed and are reported. Potential biases in the 532-nm parallel calibration appear to be small but are still under investigation. The calibration of the 532-nm perpendicular channel relative to the 532-nm parallel appears to be quite accurate. Thus, volume depolarization ratios should be quite reliable. Uncertainties in the 1064-nm channel calibration have not been studied as thoroughly. There do not appear to be gross errors in 1064-nm calibration, but biases on the order of 10% are not unexpected.

Data Quality Statement for the Transient Response of the 532 nm Detectors

Data Release Version: 1.10
Data Release Date: December 8, 2006
Document Revision Date: December 8, 2006

Introduction

This document provides a high-level quality assessment of the lidar 532 nm detector response. As such, it represents the minimum information needed by scientists and researchers for appropriate and successful use of

the lidar level 1 and 2 data products. We strongly suggest that all authors, researchers, and reviewers of research papers review this document for the latest status before publishing any scientific papers using lidar data products.

The purpose of these data quality summaries is to inform users of the accuracy of CALIOP data products as determined by the CALIPSO Science Team and Lidar Science Working Group (LSWG). This document is intended to briefly summarize key validation results; provide cautions in those areas where users might easily misinterpret the data; supply links to further information about the data products and the algorithms used to generate them; and offer information about planned algorithm revisions and data improvements.

Additional Resources

- Hunt, W. H, D. M. Winker, M. A. Vaughan, K. A. Powell, P. L. Lucker, and C. Weimer, 2009: CALIPSO Lidar Description and Performance Assessment, *J. Atmos. Oceanic Technol.*, **26**, 1214–1228, https://doi.org/10.1175/2009JTECHA1223.1.
- Lu, X., Y. Hu, M. Vaughan, S. Rodier, C. Trepte, P. Lucker, and A. Omar, 2020: New attenuated backscatter profile by removing the CALIOP receiver's transient response, *JQSRT*, **255**, 107244, https://doi.org/10.1016/j.jqsrt.2020.107244.
- McGill, M. J., M. A. Vaughan, C. R. Trepte, W. D. Hart, D. L. Hlavka, D. M. Winker, and R. Kuehn, 2007: Airborne validation of spatial properties measured by the CALIPSO lidar, *J. Geophys. Res.*, **112**, D20201, https://doi.org/10.1029/2007JD008768.
- Ryan, R. A., M. A. Vaughan, S. D. Rodier, J. L. Tackett, J. A. Reagan, R. A. Ferrare, J. W. Hair, and B. J. Getzewich, 2024: Total Column Optical Depths Retrieved from CALIPSO Lidar Ocean Surface Backscatter, *Atmos. Meas. Tech.*, **17**, 6517–6545, https://doi.org/10.5194/amt-17-6517-2024.

Appendix 1: Granules Containing Unusual Off-Nadir Angles

Table 13: During the mission, CALIOP conducted an intermittent series of measurements to characterize ocean surface backscatter at high off-nadir angles (i.e., greater than ~10°). This table lists the start time, measurement duration, and minimum and maximum off-nadir angles for each measurement. Granules containing these data are not part of the standard lidar level 1b data set.

Start Date/Time	duration (min)	θ_{min}	θ_{max}
2006-06-15@11:17:59 UTC	46.569	0.002	42.935
2007-08-21@20:42:00 UTC	41.085	3.181	29.943
2007-11-28@20:19:12 UTC	41.502	3.167	29.945
2008-02-07@10:05:30 UTC	45.863	0.025	45.813
2008-04-29@08:24:29 UTC	45.442	0.007	45.703
2009-11-24@10:06:45 UTC	45.902	0.029	45.812
2014-01-28@11:05:59 UTC	4.383	N/A	N/A
2014-07-17@13:36:28 UTC	52.217	N/A	N/A
2015-09-23@10:55:03 UTC	48.375	3.000	20.000
2015-10-07@12:45:12 UTC	45.120	3.000	20.000
2015-11-25@08:25:55 UTC	46.226	0.029	45.806
2015-10-21@11:17:13 UTC	44.252	3.087	29.997
2015-11-04@13:07:06 UTC	41.335	3.077	30.036
2015-11-18@11:39:15 UTC	43.418	3.042	30.063
2015-12-02@11:51:04 UTC	42.668	3.013	30.090

Start Date/Time	duration (min)	θ_{min}	θ_{max}
2015-12-16@12:03:01 UTC	42.335	3.013	30.107
2016-01-13@12:29:05 UTC	41.585	2.981	30.109
2016-01-27@14:20:06 UTC	41.252	2.985	30.109
2016-03-30@13:44:06 UTC	40.918	3.011	30.108
2016-04-13@13:58:04 UTC	42.668	2.995	30.104
2016-04-27@14:13:11 UTC	43.252	3.151	29.985
2016-05-11@12:48:05 UTC	42.668	3.146	29.953
2016-05-25@14:39:07 UTC	41.585	3.164	29.944
2016-06-08@11:34:13 UTC	41.502	3.162	29.939
2016-06-22@13:25:14 UTC	42.502	3.175	29.945
2016-07-13@10:25:06 UTC	41.585	3.161	29.943
2016-07-27@04:02:12 UTC	41.252	3.181	29.936
2016-08-10@04:13:00 UTC	41.418	3.182	29.941
2016-08-24@04:24:05 UTC	41.418	3.165	29.944
2016-09-07@02:56:15 UTC	41.085	3.147	29.997
2016-09-21@03:07:03 UTC	41.585	3.147	29.997
2016-10-19@03:29:05 UTC	40.168	3.096	30.062
2016-11-09@03:44:03 UTC	41.585	3.027	30.096
2016-11-30@04:02:03 UTC	40.418	3.021	30.108
2016-12-14@04:14:09 UTC	40.252	3.022	30.107
2017-01-11@03:00:08 UTC	41.085	3.024	30.105
2017-01-25@11:28:10 UTC	41.085	3.022	14.104
2017-02-08@13:20:12 UTC	41.502	2.031	14.091
2017-02-22@11:55:06 UTC	41.002	3.064	14.069
2017-03-08@12:09:04 UTC	41.502	3.088	10.036
2017-03-22@12:23:11 UTC	41.585	3.118	10.004
2017-04-19@12:51:07 UTC	41.585	3.152	9.948
2017-05-03@13:04:04 UTC	41.002	3.165	9.948
2017-05-17@11:39:15 UTC	41.085	3.159	9.947
2017-05-23@07:45:59 UTC	42.667	3.185	45.611
2018-11-28@10:07:06 UTC	56.085	2.956	41.013
2019-05-03@13:53:02 UTC	41.252	3.164	44.940
2020-05-27@20:47:45 UTC	44.280	2.973	27.323
2021-11-23@14:05:59 UTC	45.557	0.031	45.996

Table 14: The mission collected a series of extended measurements in 2017 at off-nadir angles of 1.0, 1.5 and 2.0° to assess the impacts on horizontally oriented ice detection (Avery et al., 2020). These granules are included in the standard level 1b data set.

Start Date/Time	End Date/Time	θ
2017-02-03@00:00:25 UTC	2017-02-08@13:20:40 UTC	2.0°

Start Date/Time	End Date/Time	θ
2017-02-22@12:35:31 UTC	2017-02-28@15:53:21 UTC	1.0°
2017-06-22@21:54:14 UTC	2017-06-26@13:50:44 UTC	1.5°

Appendix 2: Estimating Random Uncertainties for Attenuated Backscatter Coefficients

Zhaoyan Liu, CALIPSO Lidar Science Working Group, NASA Ames Research Center

To keep CALIOP lidar level 1b (L1B) file sizes within manageable limits, the range-resolved uncertainties for the attenuated backscatter coefficients, β′(r), are not explicitly reported in the L1B data product, as doing so would approximately double the (already large) file sizes. What is included in the L1B files are all the instrument parameters needed to compute the variance of the height-resolved attenuated backscatter coefficients. The variance calculation is

$$\mathrm{var}\big(\beta'(k,r_i)\big) = \left(\frac{{r_i}^2 \cdot \mathrm{NSF}^2(k) \cdot \beta'(k,r_i)}{E \cdot C(k)} + \left(\frac{{r_i}^2 \cdot \mathrm{RMS}(k)}{E \cdot G_A \cdot C(k)}\right)^2\right)\left(\frac{f_{\mathrm{correct}}^2(N_{\mathrm{bin}}(r_i), N_{\mathrm{shift}})}{N_{\mathrm{bin}}(r_i) \cdot N_{\mathrm{shot}}}\right). \quad (1)$$

The uncertainty in the attenuated backscatter coefficient, Δβ′(z), is the square root of var(β′(z)). The index k indicates the kth profile in an along-track sequence of profiles and r_i is the range from the CALIPSO satellite to the ith altitude bin ($r_i = (H - z_i)/\cos(\theta)$, where H is the satellite altitude and θ is the off-nadir angle). NSF is the noise scale factor for the profile, E is the laser energy, C is the calibration coefficient, G_A is the gain of the amplifier, and RMS is the random noise of the background signal, including detector dark current, background radiation, etc. Table 15 lists the SDSs in the L1B product containing each of these parameters. N_{bin} and N_{shot} are, respectively, the number of range bins and number of laser shots averaged for the different CALIPSO data averaging regimes, as shown in Table 16.

Table 15: SDSs in the CALIOP L1B data files containing the parameters used in equation (1)

parameter	SDS name
z_i	Lidar_Data_Altitudes
H	Spacecraft_Altitude
θ	Off_Nadir_Angle
NSF	Noise_Scale_Factor_532_Parallel, Noise_Scale_Factor_532_Perpendicular, or Noise_Scale_Factor_1064
E	Laser_Energy_532
C	Calibration_Constant_532 (parallel channel), Calibration_Constant_532 × Depolarization_Gain_Ratio_532 (perpendicular channel), or Calibration_Constant_1064
G_A	Parallel_Amplifier_Gain_532, Perpendicular_Amplifier_Gain_532, or Amplifier_Gain_1064
β′(k, r)	Total_Attenuated_Backscatter_532 – Perpendicular_Attenuated_Backscatter_532, Perpendicular_Attenuated_Backscatter_532, or Attenuated_Backscatter_1064
N_{shift}	Number_Bins_Shift
N_{bin}	See Table 16
N_{shot}	See Table 16
$f_{correct}$	See Table 17

$f_{correct}$ is a correction factor used to account for the partial correlation among neighboring samples in a raw Level 0 (L0) profile (Liu et al., 2006; Vaillant de Guélis et al., 2021), and additional correlation due to data redistribution in the altitude registration of L0 data samples during the L1 processing (Powell et al., 2009). The integral time of the amplifier of the lidar receiver is slightly longer than 0.02 ms (30 meters in distance) and is larger than the onboard sampling interval (15 m), causing the downlinked data (averaged over different numbers of 15-m samples for different altitude ranges as listed in Table 16) to be partially correlated. In addition, there may be an offset in the altitude registration of a profile due to the variation of the nadir viewing angle of the lidar system. The L0 signal profiles received at the ground are averaged vertically and horizontally (i.e., as in Table 16) prior to downlink and exhibit some jitter in altitude registration because of inexact onboard ephemeris data. To correct the altitude registration and geolocation, the profiles are first expanded to pseudo-single-shot profiles with 30-m vertical sample spacing, replicating data values as necessary where the downlink resolution is greater than 30 meters vertically and one shot horizontally. Each reconstituted profile is then geolocated and the altitude of each sample is computed. Based on the computed altitudes, the samples are mapped onto a fixed-altitude array and averaged back to the altitude dependent downlink resolutions (Powell et al., 2009). In the -0.5 km to 8.2 km altitude range (zero-based altitude indices of 288 – 577), data values are simply shifted to the appropriate range/altitude bins, because the bin size for this altitude range is 30 meters. For the other altitude ranges whose bin size is larger than 30 meters (60 to 300 meters), the shift is accomplished by regridding then reaveraging the L0 data, thus redistributing the magnitudes of neighboring data samples, and thereby introducing additional correlation in the L1 data. N_{shift} denotes the number of 15-m bins shifted. $f_{correct}$ can then be computed using

$$f_{correct}(\mathrm{N_{bin}}, \mathrm{N_{shift}}) = \left(\begin{array}{c} \mathrm{g}^2(\mathrm{N_{bin}}) \left(\left(\frac{\mathrm{N_{bin}} - \mathrm{N_{shift}}}{\mathrm{N_{bin}}} \right)^2 + \left(\frac{\mathrm{N_{shift}}}{\mathrm{N_{bin}}} \right)^2 \right) + \\ 2 \left(\frac{\mathrm{N_{shift}}(\mathrm{N_{bin}} - \mathrm{N_{shift}})}{{\mathrm{N_{bin}}}^2} \right) \left(\sum_{\mathrm{m}=1}^{\mathrm{N_{bin}}} \frac{\mathrm{m}}{\mathrm{N_{bin}}} \mathrm{R(m)} + \sum_{\mathrm{m}=1}^{\mathrm{N_{bin}}-1} \frac{\mathrm{N_{bin}} - \mathrm{m}}{\mathrm{N_{bin}}} \mathrm{R}(\mathrm{N_{bin}} + \mathrm{m}) \right) \end{array} \right)^{\frac{1}{2}} \quad (2)$$

where

$$g(\mathrm{N_{bin}}) = \left(1 + 2 \sum_{m=1}^{\mathrm{N_{bin}}-1} \left(\frac{\mathrm{N_{bin}} - \mathrm{m}}{\mathrm{N_{bin}}} \right) \mathrm{R(m)} \right)^{\frac{1}{2}} \quad (3)$$

with R() representing the autocorrelation coefficients (Liu et al., 2006). The computed $f_{correct}$ values are given in Table 17, using the R values determined based on the prelaunch lab experiment data.

In practice, caution should be paid in using equation (1) to calculate the uncertainty for single-shot profiles, because single-shot data are very noisy and, for large negative excursions of $\beta'(k, r_i)$, may result in an attempt to take the square root of a negative value.

Table 16: Numbers of 15-m range bins and laser shots averaged for different altitude ranges in L1B data products

Altitude range (km)	Altitude index range	532 nm		1064 nm	
		N_{bin}	N_{shot}	N_{bin}	N_{shot}
40.0 – 30.1	0-32	20	15	N/A	N/A
30.1 – 20.2	33-87	12	5	12	5
20.2 – 8.3	88-287	4	3	4	3
8.3 – -0.5	288-577	2	1	4	1
-0.5 – -2.0	578-582	20	1	20	1

Table 17: $f_{correct}$ for different altitude ranges and numbers of 30-meter bins shifted

	N_{shift}	Remark

Bin index	0	1	2	3	4	5	6	7	8	9	10	
0-32	1.596	1.448	1.322	1.224	1.161	1.140	1.161	1.224	1.322	1.448	1.596	Cycle of 10
33-87	1.573	1.345	1.188	1.131	1.188	1.345	1.573	1.345	1.188	1.130	1.188	Cycle of 6
88-287	1.451	1.080	1.451	1.080	1.451	1.080	1.451	1.080	1.451	1.080	1.451	Cycle of 2
288-577	1.269 1.451	1.269 1.451	1.269 1.451	1.269 1.451	1.269 1.451	1.269 1.451	1.269 1.451	1.269 1.451	1.269 1.451	1.269 1.451	1.269 1.451	532 nm 1064 nm
578-582	1.596	1.448	1.322	1.224	1.161	1.140	1.161	1.224	1.322	1.448	1.596	Cycle of 10

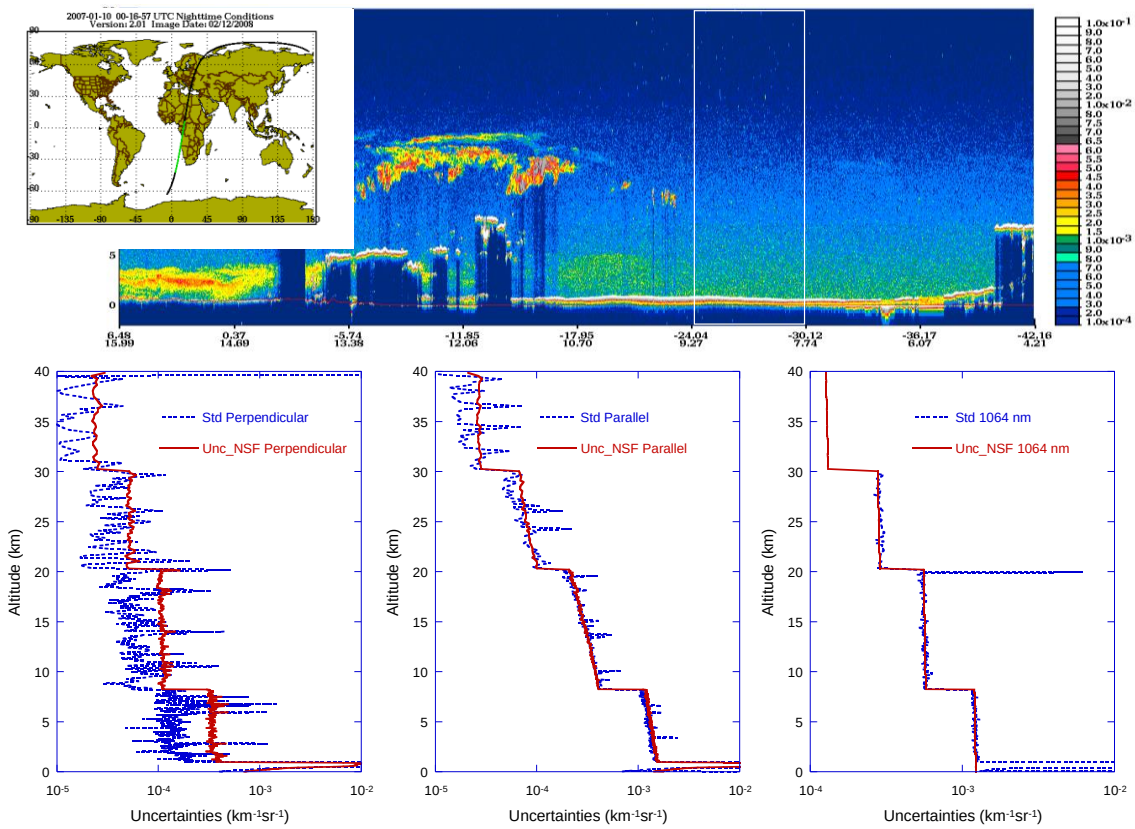

Figure 1: Random uncertainties computed using equation (1) for a nighttime CALIOP data segment passing over the southern Atlantic Ocean on 10 January 2007, as indicated by the white box in the upper browse image. The lower row of images show uncertainty estimates for the 532 nm perpendicular (left panel) and parallel (middle panel) channels and the 1064 nm channel (right panel). The red lines represent the means of the uncertainties calculated using equation (1) while the blue lines show the standard deviations of the single-shot profiles. Good

agreement is seen in the NSF-estimated uncertainties and standard deviations, except in the 532-nm perpendicular signal and the upper part of the 532-nm parallel signal where the return signal is very weak.

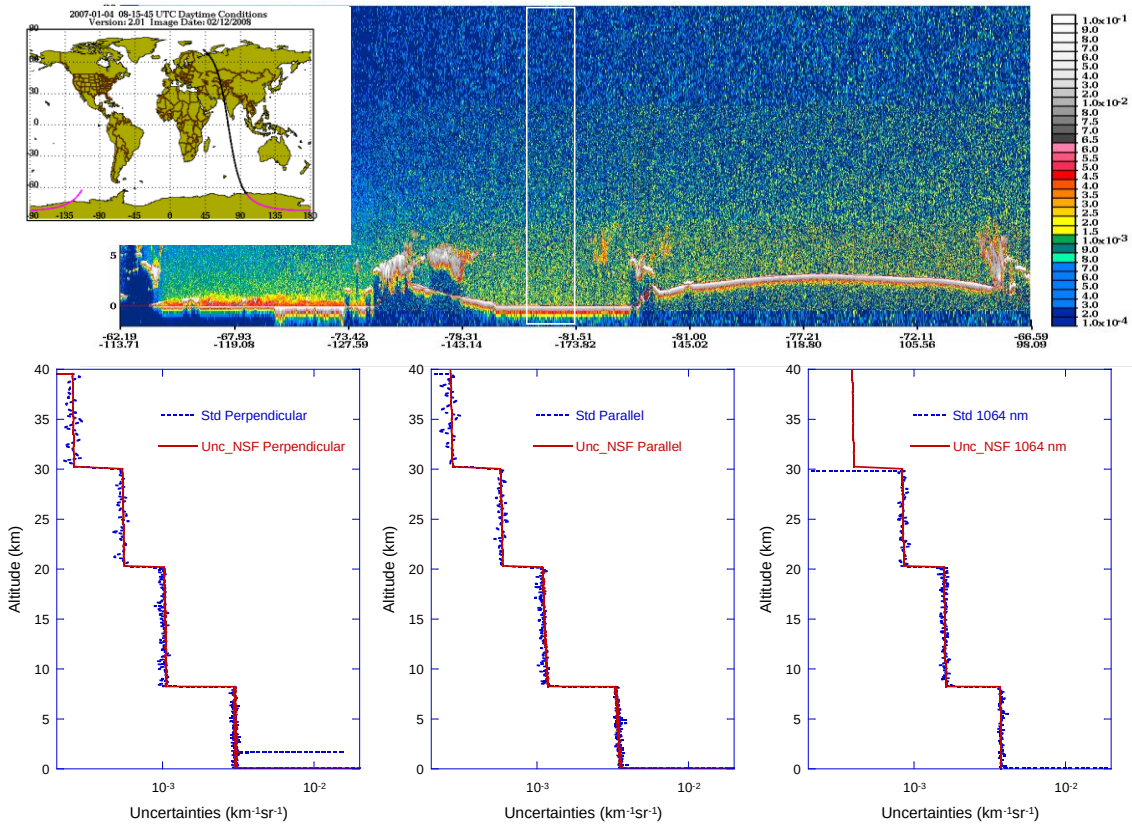

Figure 2: Same as Figure 1, but for a daytime data passing over Antarctica on 10 January 2007. The correspondence between the NSF-estimated uncertainties and the associated standard deviations is greatly improved in the 532 nm channel due to the high backgrounds value (corresponding to large RMS baseline value) caused by sunlight reflected from the ice-covered surface.

Appendix 3: Non-ideal Response of the CALIOP 532 nm Detectors

Initial Release: 8 December 2006
Last Update: 5 October 2025

The detectors for CALIOP's 532 nm channels were photomultiplier tubes (PMTs), while the 1064 nm detector was an avalanche photodiode (Hunt et al., 2009). At 532 nm, both the parallel and perpendicular channels exhibited a non-ideal recovery of the lidar signal after a very strong backscattering target was observed. Examples of very strong backscattering targets are water clouds and surface returns. PMT after-pulsing (ionization of residual gas) is the likely cause of this non-ideal transient recovery (Hamamatsu, 2017). This effect is well documented in the literature for photon counting applications. The time scale of the effect is dependent on PMT voltage, gas species, and PMT internal geometry. It is also possible that the non-ideal transient recovery is what is commonly called signal induced noise (Acharya et al., 2004). It is unlikely that the lidar receiver electronics are the source of the problem because the 1064 nm channel uses a similar design and performed well throughout the mission.

Figure A3-1 shows browse images of total attenuated backscatter at 532 nm (top) and 1064 nm (bottom). In strongly scattering targets – e.g., the stratus deck on the left and the Antarctic surface on the right – the non-ideal transient recovery in the 532 nm image appears as a gradual transition of colors from very high attenuated backscatter values (white) to lower but still elevated values (yellow). In contrast, in the 1064 nm image, where the detector response is normal, and these features appear as an almost solid bands of white. This is especially visible

over the Antarctic ice sheet. For both wavelengths, the vertical extents of the cirrus clouds are essentially identical, demonstrating that in less robust features there is little, if any, contribution to the 532 nm signals from the non-ideal detector response.

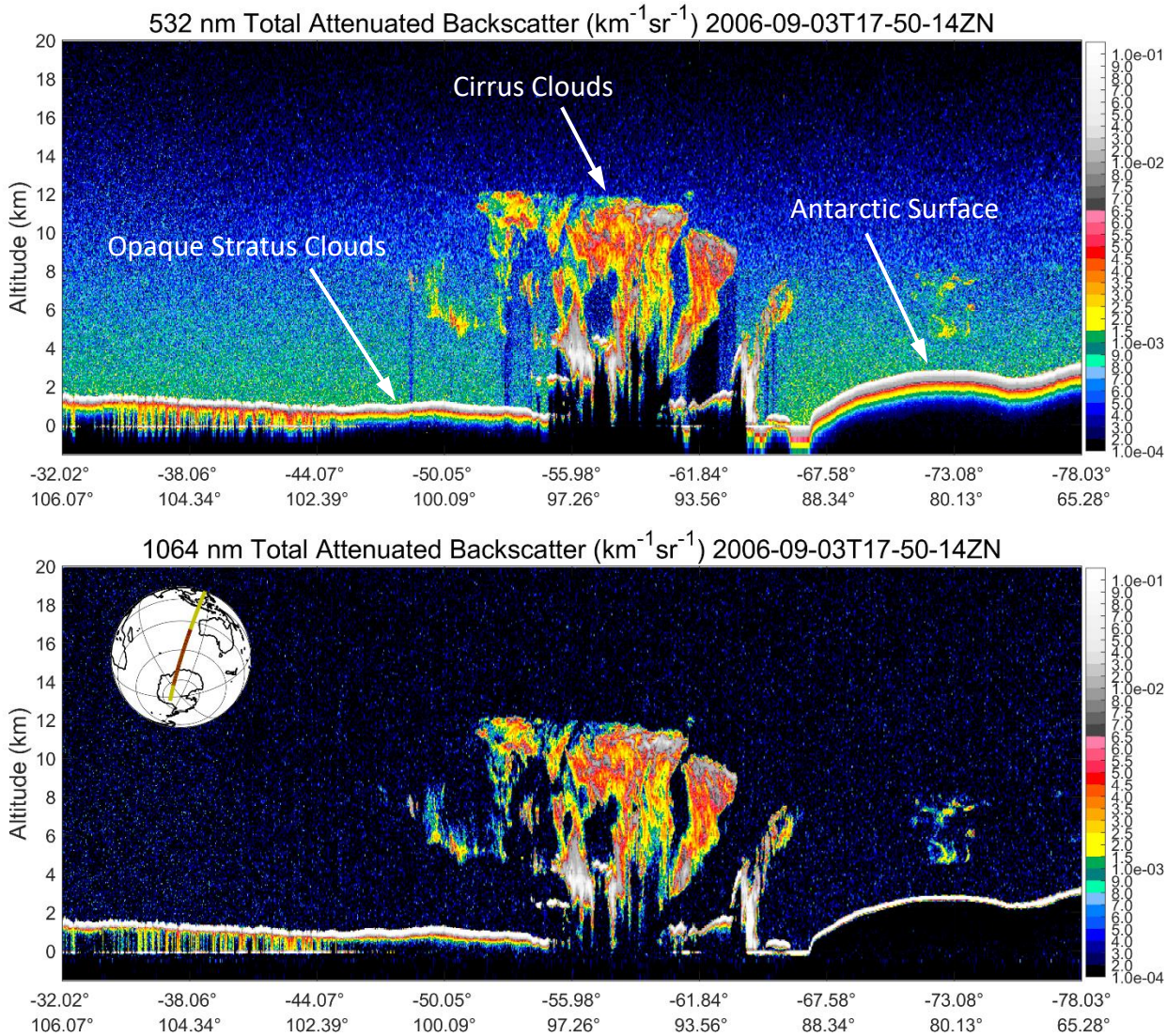

Figure A3-1: 532 nm (top panel) and 1064 nm (bottom panel) total attenuated backscatter coefficients measured on 2006-09-03 over the southern Pacific Ocean and extending into Antarctic. The difference in transient response between the two channels is most prominent over the Antarctic ice sheets, where the 532 nm signal shows a non-ideal response that appears to penetrate over 1 km below the surface whereas the 1064 nm signal is normal for space-based measurements of hard targets.

Prior to launch (2002), a series of laboratory measurements of the flight hardware was conducted to characterize the responses of both the 532 nm parallel and perpendicular channel detectors. In 87 separate tests, dense clouds were simulated using square waves of varying amplitude and duration. Surface returns could also be used to characterize the detector response assuming the peak signal did not saturate the low-gain digitizer and there is sufficient time between the onset of the simulated surface return and the last range bin digitized in the receiver. Initial analyses demonstrated that the non-ideal recovery behaves like an after-pulse signal, with the observed response being a function of both the signal amplitude and duration.

A Richardson-Lucy deconvolution algorithm was applied to the lab measurements to retrieve the instrument response function. The assumed true signal in these calculations was a square wave with a temporal duration

equal to the detector illumination used time in each test. Figure A3-2 shows the retrieved response functions from the 532 nm parallel channel detector for various lighting conditions (i.e., different pulse amplitudes and widths).

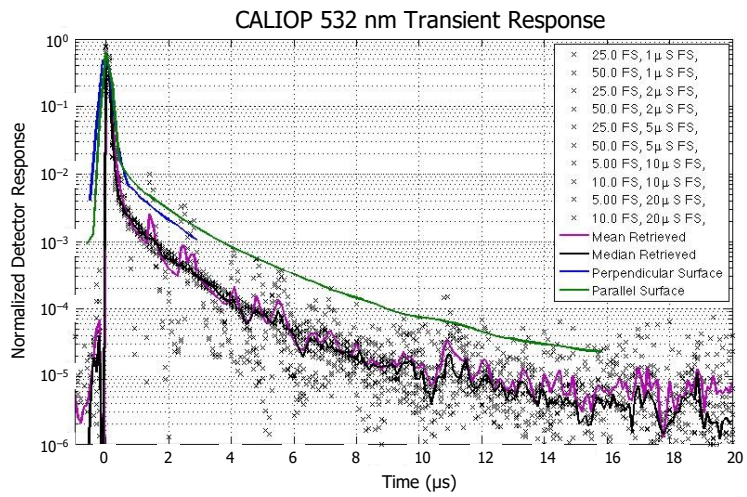

Figure A3-2: Test data using square waves with different pulse amplitudes and widths to characterize the non-ideal response of the 532 nm detectors. The non-ideal response is the approximately exponential decay (i.e., "noise tail") beginning at ~0.7 μs. Mean values for different tests are shown using solid lines. Simulations from surface returns that use the strongest signals show noise tails that extend longer and are greater in magnitude than cloud simulations using less intense inputs.

Very early in the mission, the CALIPSO project conducted a number of dedicated validation flights with the NASA Langley High Spectral Resolution Lidar (HSRL; Hair et al., 2008) to help characterize the on-orbit behavior of the 532 nm detectors. Figure A3-3 shows selected results from these comparisons. The left panel shows measurements of transparent water clouds. Time from exact coincidence of the two sensors is approximately 30 minutes. The non-ideal response of the CALIOP detectors is seen in the decaying portion of lidar signal that extends from ~3.1 km to ~1.0 km. While illustrative, the comparison is somewhat inexact because the water cloud top altitude changed between the observation times. Furthermore, the CALIPSO and HSRL viewing geometries are considerably different, and there is a significant contribution from multiple scattering in the CALIPSO observations (Hu et al., 2009). The right panel of Figure A3-3 shows measurements of an aerosol layer acquired closer to the exact coincident time. This comparison demonstrates that the effect of the non-ideal transient response within weaker scattering layers is negligible. McGill et al., 2007 shows additional detection comparisons for cirrus clouds measured by CALIOP and the Cloud Physics Lidar.

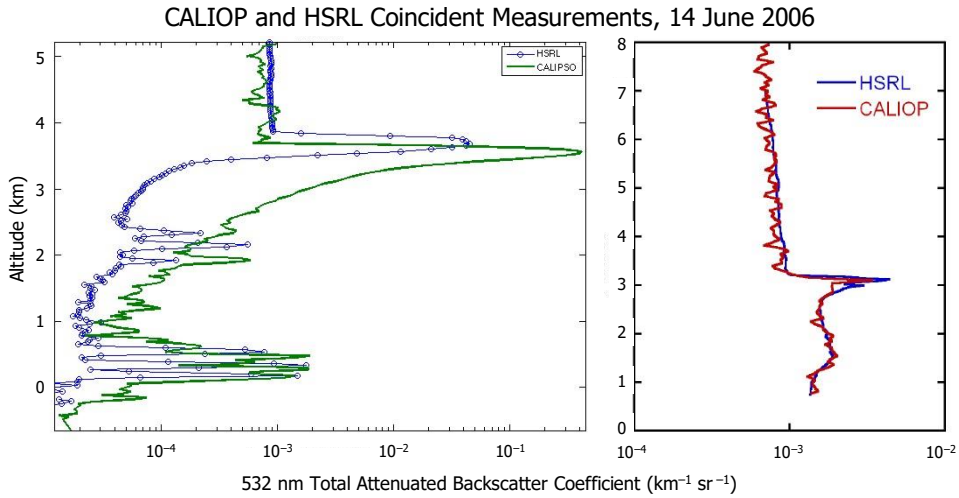

Figure A3-3: The left panel shows a comparison of water clouds measurements by CALIOP and the LaRC HSRL. The slight offset in cloud top heights is due to a 30-minute temporal mismatch between the two sensors. The non-ideal noise tail in the CALIOP measurement of the upper layer extends from ~3.1 km to ~1.0 km. The right panel shows measurements of an aerosol layer acquired closer to the exact coincidence between the two lidars. Detector noise tails are not at all evident in this more weakly scattering feature.

In the CALIOP level 2 analyses, this non-ideal detector response can cause errors in the estimates of the lower layer boundaries in atmospheric features (Vaughan et al., 2009). In particular, the apparent bases of opaque water clouds may appear to extend further toward the surface than would otherwise be expected. However, this error is largely inconsequential, since CALIOP cannot accurately measure the true base altitudes of opaque layers. A comprehensive study by Lu et al., 2020 suggests that these unwanted detector transients can be expected for any target in which the peak attenuated backscatter exceeds 0.01 km^{-1} sr^{-1} (e.g., the left panel of Figure A3-3). Below that limit, as seen in the right panel of Figure A3-3, non-ideal response effects on CALIOP's layer detection scheme can largely be ignored, as they introduce vertical extent errors of no more than 2%, with error magnitude decreasing as a function of feature backscatter intensity.

References

Acharya, Y. B., S. Sharma and H. Chandra, 2004: Signal induced noise in PMT detection of lidar signals, *Measurement*, **35**, 269–276, https://doi.org/10.1016/j.measurement.2003.11.003.

Avery, M. A., R. A. Ryan, B. J. Getzewich, M. A. Vaughan, D. M. Winker, Y. Hu, A. Garnier, J. Pelon and C. A. Verhappen, 2020: CALIOP V4 Cloud Thermodynamic Phase Assignment and the Impact of Near-Nadir Viewing Angles, *Atmos. Meas. Tech.*, **13**, 4539-4563, https://doi.org/10.5194/amt-13-4539-2020.

Campbell, J. R., M. A. Vaughan, M. Oo, R. E. Holz, J. R. Lewis, and E. J. Welton, 2015: Distinguishing cirrus cloud presence in autonomous lidar measurements, *Atmos. Meas. Tech.*, **8**, 435–449, https://doi.org/10.5194/amt-8-435-2015.

Doelling, D., D. Morstad, B. R. Scarino, R. Bhatt, and A. Gopalan, 2013: The Characterization of Deep Convective Clouds as an Invariant Calibration Target and as a Visible Calibration Technique, *IEEE Trans. Geosci. Remote Sens.*, **51**, 1147–1159, https://doi.org/10.1109/TGRS.2012.2225066.

Gelaro, R. and 30 coauthors, 2017: The Modern-Era Retrospective Analysis for Research and Applications, Version 2 (MERRA-2), *J. Climate*, **30**, 5419–5454, https://doi.org/10.1175/JCLI-D-16-0758.1.

Getzewich, B. J., M. A. Vaughan, W. H. Hunt, M. A. Avery, K. A. Powell, J. L. Tackett, D. M. Winker, J. Kar, K.-P. Lee, and T. Toth, 2018: CALIPSO Lidar Calibration at 532-nm: Version 4 Daytime Algorithm, *Atmos. Meas. Tech.*, **11**, 6309–6326, https://doi.org/10.5194/amt-11-6309-2018.

Gueymard, C. A., 2018: Revised composite extraterrestrial spectrum based on recent solar irradiance observations, *Solar Energy*, **169**, 434–440, https://doi.org/10.1016/j.solener.2018.04.067.

Hair, J. W., C. A. Hostetler, A. L. Cook, D. B. Harper, R. A. Ferrare, T. L. Mack, W. Welch, L. R. Izquierdo, and F. E. Hovis, 2008: Airborne High Spectral Resolution Lidar for profiling aerosol optical properties, *Appl. Opt.*, **47**, 6734-6752, https://doi.org/10.1364/AO.47.006734.

Hamamatsu Photonics Editorial Committee, 2017: Photomultiplier Tubes – Basics and Applications, 4th Edition, Hamamatsu Photonics K. K. Electron Tube Division, 332 pp; available at https://www.hamamatsu.com/content/dam/hamamatsu-photonics/sites/documents/99_SALES_LIBRARY/etd/PMT_handbook_v4E.pdf.

Hu, Y., D. Winker, M. Vaughan, B. Lin, A. Omar, C. Trepte, D. Flittner, P. Yang, W. Sun, Z. Liu, Z. Wang, S. Young, K. Stamnes, J. Huang, R. Kuehn, B. Baum, and R. Holz, 2009: CALIPSO/CALIOP Cloud Phase Discrimination Algorithm, *J. Atmos. Oceanic Technol.*, **26**, 2293–2309, https://doi.org/10.1175/2009JTECHA1280.1.

Hunt, W. H, D. M. Winker, M. A. Vaughan, K. A. Powell, P. L. Lucker, and C. Weimer, 2009: CALIPSO Lidar Description and Performance Assessment, *J. Atmos. Oceanic Technol.*, **26**, 1214–1228, https://doi.org/10.1175/2009JTECHA1223.1.

Kar, J., M. A. Vaughan, K. P. Lee, J. Tackett, M. Avery, A. Garnier, B. Getzewich, W. Hunt, D. Josset, Z. Liu, P. Lucker, B. Magill, A. Omar, J. Pelon, R. Rogers, T. D. Toth, C. Trepte, J-P. Vernier, D. Winker, and S. Young, 2018: CALIPSO Lidar Calibration at 532 nm: Version 4 Nighttime Algorithm, *Atmos. Meas. Tech.*, **11**, 1459–1479, https://doi.org/10.5194/amt-11-1459-2018.

Liu, Z., M. J. McGill, Y. Hu, C. A. Hostetler, M. Vaughan, and D. Winker, 2004: Validating lidar depolarization calibration using solar radiation scattered by ice clouds, *IEEE Geosci. Remote Sens. Lett.*, **1**, 157–161, https://doi.org/10.1109/LGRS.2004.829613.

Liu, Z., W. Hunt, M. Vaughan, C. Hostetler, M. McGill, K. Powell, D. Winker, and Y. Hu, 2006: Estimating Random Errors Due to Shot Noise in Backscatter Lidar Observations, *Appl. Opt.*, **45**, 4437–4447, https://doi.org/10.1364/AO.45.004437.

Lu, X., Y. Hu, M. Vaughan, S. Rodier, C. Trepte, P. Lucker, and A. Omar, 2020: New attenuated backscatter profile by removing the CALIOP receiver's transient response, *JQSRT*, **255**, 107244, https://doi.org/10.1016/j.jqsrt.2020.107244.

Lu, X., Y. Hu, A. Omar, R. Baize, M. Vaughan, S. Rodier, J. Kar, B. Getzewich, P. Lucker, C. Trepte, C. Hostetler and D. Winker, 2021: Global ocean studies from CALIOP/CALIPSO by removing polarization crosstalk effects, *Remote Sens.*, ***13***, 2769, https://doi.org/10.3390/rs13142769.

McGill, M. J., M. A. Vaughan, C. R. Trepte, W. D. Hart, D. L. Hlavka, D. M. Winker, and R. Kuehn, 2007: Airborne validation of spatial properties measured by the CALIPSO lidar, *J. Geophys. Res.*, **112**, D20201, https://doi.org/10.1029/2007JD008768.

Noel, V., H. Chepfer, C. Hoareau, M. Reverdy and G. Cesana, 2014: Effects of solar activity and geomagnetic field on noise in CALIOP profiles above the South Atlantic Anomaly, *Atmos. Meas. Tech.*, **7**, 1597–1603, https://doi.org/10.5194/amt-7-1597-2014.

Powell, K. A., C. A. Hostetler, Z. Liu, M. A. Vaughan, R. E. Kuehn, W. H. Hunt, K. Lee, C. R. Trepte, R. R. Rogers, S. A. Young, and D. M. Winker, 2009: CALIPSO Lidar Calibration Algorithms: Part I - Nighttime 532 nm Parallel Channel and 532 nm Perpendicular Channel, *J. Atmos. Oceanic Technol.*, **26**, 2015–2033, https://doi.org/10.1175/2009JTECHA1242.1.

Powell, K. A., M. A. Vaughan, R. R. Rogers, R. E. Kuehn, W. H. Hunt, K-P. Lee, and T. D. Murray, 2010: The CALIOP 532-nm Channel Daytime Calibration: Version 3 Algorithm, 25th International Laser Radar Conference (ILRC), 5–9 July 2010, St. Petersburg, Russia; see https://www.researchgate.net/publication/391011856.

Sassen, K., V. K. Kayetha and J. Zhu, 2012: Ice cloud depolarization for nadir and off-nadir CALIPSO measurements, *Geophys. Res. Lett.*, **39**, L20805, https://doi.org/10.1029/2012GL053116.

Tackett, J. L., R. A. Ryan, A. E. Garnier, J. Kar, B. Getzewich, X. Cai, M. A. Vaughan, C. R. Trepte, R. Verhappen, D. M. Winker and K.-P. A. Lee, 2025: Mitigating Impacts of Low Energy Laser Pulses on CALIOP Data Products, *EGUsphere* [AMTD], https://doi.org/10.5194/egusphere-2025-2376.

Tanelli, S., G. Dobrowalski, M. Lebsock, S. L. Durden, P. Partain, D. Reinke, and D. Reinke, 2014: CloudSat's Cloud Profiling Radar: Status, Performance, and latest data product changes, CALIPSO-CloudSat Science Team Meeting, 3–5 November 2014, Alexandria, VA, USA.

Vaillant de Guélis, T., M. A. Vaughan, D. M. Winker, and Z. Liu, 2021: Two-dimensional and multi-channel feature detection algorithm for the CALIPSO lidar measurements, *Atmos. Meas. Tech.*, **14**, 1593–1613, https://doi.org/10.5194/amt-14-1593-2021.

Vaillant de Guélis, T., J. L. Tackett, and D. M. Winker, 2025: A proposal for improved colorbars for cloud and aerosol lidar parameters, 31st International Laser Radar Conference, 23–28 June 2024, Landshut, Bavaria, Germany; https://ntrs.nasa.gov/citations/20240005619.

Vaughan, M. A., Z. Liu, M. J. McGill, Y. Hu, and M. D. Obland, 2010: On the Spectral Dependence of Backscatter from Cirrus Clouds: Assessing CALIOP's 1064 nm Calibration Assumptions Using Cloud Physics Lidar Measurements, *J. Geophys. Res.*, **115**, D14206, https://doi.org/10.1029/2009JD013086.

Vaughan, M., A. Garnier, D. Josset, M. Avery, K.-P. Lee, Z. Liu, W. Hunt, J. Pelon, Y. Hu, S. Burton, J. Hair, J. Tackett, B. Getzewich, J. Kar, and S. Rodier, 2019: CALIPSO Lidar Calibration at 1064 nm: Version 4 Algorithm, *Atmos. Meas. Tech.*, **12**, 51–82, https://doi.org/10.5194/amt-12-51-2019.

Vaughan, M., S. D. Rodier, Z. Liu, A. Garnier, K.-P. Lee, B. Getzewich and S. Zeng, 2023: Correcting CALIOP Polarization Gain Ratios for Diurnal Variations, in Proceedings of the 30th International Laser Radar Conference, Sullivan, J. T., T. Leblanc, S. Tucker, B. Demoz, E. Eloranta, C. Hostetler, S. Ishii, L. Mona, F. Moshary, A. Papayannis and K. Rupavatharam, Eds., pp. 691–697, Springer Atmospheric Sciences, Springer, Cham., https://doi.org/10.1007/978-3-031-37818-8_89.

Vernier, J. P., J. P. Pommereau, A. Garnier, J. Pelon, N. Larsen, J. Nielsen, T. Christensen, F. Cairo, L. W. Thomason, T. Leblanc and I. S. McDermid, 2009: The tropical stratospheric aerosol layer from CALIPSO lidar observations, *J. Geophys. Res.*, **114**, D00H10, https://doi.org/10.1029/2009JD011946.

Winker, D. M., M. A. Vaughan, A. H. Omar, Y. Hu, K. A. Powell, Z. Liu, W. H. Hunt, and S. A. Young, 2009: Overview of the CALIPSO Mission and CALIOP Data Processing Algorithms, *J. Atmos. Oceanic Technol.*, **26**, 2310–2323, https://doi.org/10.1175/2009JTECHA1281.1.